Article

Genome-wide CRISPR screen in human T cells reveals regulators of FOXP3

https://doi.org/10.1038/s41586-025-08795-5

Received: 8 September 2023

Accepted: 14 February 2025

Published online: 26 March 2025

Check for updates

Kelvin Y. Chen[1,7]✉, Tatsuya Kibayashi[2,3,7], Ambre Giguelay[4,5], Mayu Hata[1], Shunsuke Nakajima[2,3], Norihisa Mikami[1], Yusuke Takeshima[1], Kenji Ichiyama[1], Ryusuke Omiya[2,3], Leif S. Ludwig[4,5], Kunihiro Hattori[2,3] & Shimon Sakaguchi[1,6]✉

Regulatory T (T_{reg}) cells, which specifically express the master transcription factor FOXP3, have a pivotal role in maintaining immunological tolerance and homeostasis and have the potential to revolutionize cell therapies for autoimmune diseases[1–3]. Although stimulation of naive $CD4^+$ T cells in the presence of TGFβ and IL-2 can induce $FOXP3^+$ T_{reg} cells in vitro (iT_{reg} cells), the resulting cells are often unstable and have thus far hampered translational efforts[4–6]. A systematic approach towards understanding the regulatory networks that dictate T_{reg} differentiation could lead to more effective iT_{reg} cell-based therapies. Here we performed a genome-wide CRISPR loss-of-function screen to catalogue gene regulatory determinants of FOXP3 induction in primary human T cells and characterized their effects at single-cell resolution using Perturb-icCITE-seq. We identify the RBPJ–NCOR repressor complex as a novel, context-specific negative regulator of FOXP3 expression. RBPJ-targeted knockout enhanced iT_{reg} differentiation and function, independent of canonical Notch signalling. Repeated cytokine and T cell receptor signalling stimulation in vitro revealed that RBPJ-deficient iT_{reg} cells exhibit increased phenotypic stability compared with control cells through DNA demethylation of the *FOXP3* enhancer CNS2, reinforcing FOXP3 expression. Conversely, overexpression of RBPJ potently suppressed FOXP3 induction through direct modulation of *FOXP3* histone acetylation by HDAC3. Finally, RBPJ-ablated human iT_{reg} cells more effectively suppressed xenogeneic graft-versus-host disease than control iT_{reg} cells in a humanized mouse model. Together, our findings reveal novel regulators of FOXP3 and point towards new avenues to improve the efficacy of adoptive cell therapy for autoimmune disease.

T_{reg} cells are an integral constituent of the adaptive immune system and are engaged in maintaining immunological self-tolerance[1]. Although disruption of T_{reg} function leads to autoimmune disease and immunopathology deleterious to the host, enhancement of T_{reg} function and stability holds promise for treatment and reversal of immune-mediated diseases[2,3]. Current endeavours towards achieving T_{reg}-based therapy have been directed at expanding natural T_{reg} (nT_{reg}) cells or inducing the conversion of T cells into T_{reg} cells through antigenic stimulation in the presence of TGFβ and IL-2 in vitro (iT_{reg} cells)[7,8]. Recent efforts integrating CRISPR-based approaches into the realm of T_{reg} manipulation have introduced new prospects for extending the clinical applicability of T_{reg} cells by tailoring core functional properties, such as their immunosuppressive potency, specificity and stability. Concurrently, the advent of large-scale CRISPR screens has enabled the unbiased discovery of novel regulators of T cell function and fate[9–11], but efforts thus far in T_{reg} cells have primarily focused on the maintenance and stability of nT_{reg} cells[12–14]. Here we describe unbiased genome-scale genetic screens performed on stimulated human T cells undergoing iT_{reg} conversion. We identified *RBPJ* as a context-specific negative regulator of iT_{reg} lineage conversion, and show that *RBPJ* deficiency improves the conversion, stability, maintenance and function of iT_{reg} cells through increased *FOXP3* expression, CNS2 demethylation, local histone acetylation and effector gene expression. Finally, we demonstrate that *RBPJ*-ablated iT_{reg} cells can enhance in vivo function and protect against graft-versus-host disease (GvHD) in a humanized mouse model. These findings are instrumental towards advancing our understanding of the molecular basis of T_{reg} differentiation and the development of iT_{reg}-based therapy for autoimmune and other inflammatory diseases.

CRISPR screening for regulators of FOXP3

To uncover putative regulators of FOXP3 expression, we developed a pooled CRISPR-screening platform in primary human $CD4^+$ T cells undergoing iT_{reg} differentiation (Fig. 1a). Our screening strategy was

[1]Laboratory of Experimental Immunology, Immunology Frontier Research Center, Osaka University, Osaka, Japan. [2]Joint Research Chair of Innovative Drug Discovery in Immunology, Immunology Frontier Research Center, Osaka University, Osaka, Japan. [3]Research Division, Chugai Pharmaceutical Co. Ltd, Yokohama, Japan. [4]Berlin Institute of Health at Charité–Universitätsmedizin Berlin, Berlin, Germany. [5]Max-Delbrück-Center for Molecular Medicine in the Helmholtz Association (MDC), Berlin Institute for Medical Systems Biology (BIMSB), Berlin, Germany. [6]Department of Experimental Pathology, Institute for Life and Medical Sciences, Kyoto University, Kyoto, Japan. [7]These authors contributed equally: Kelvin Y. Chen, Tatsuya Kibayashi. ✉e-mail: chenk@ifrec.osaka-u.ac.jp; shimon@ifrec.osaka-u.ac.jp

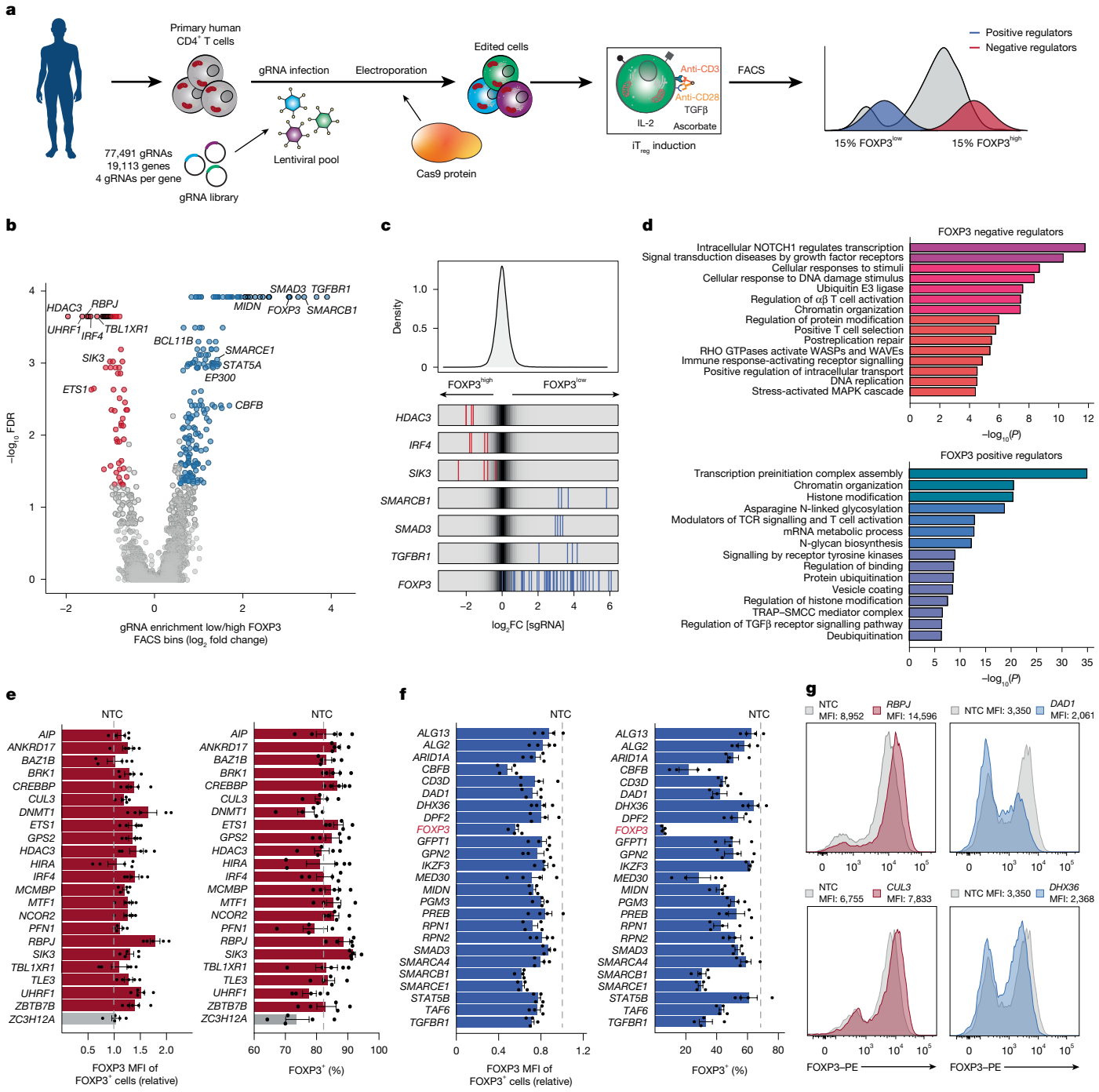

Fig. 1 | A whole-genome CRISPR screen in primary human T cells uncovers novel regulators of *FOXP3* induction. a, Schematic of pooled CRISPR screens on human iT_{reg} induction. Adapted from ref. 51, Springer Nature America, Inc. **b**, Volcano plot of the hits from the screen. The *x* axis shows the median $\log_2$ fold change (LFC) for all sgRNAs per gene, whereas the *y* axis depicts the false discovery rate (FDR). Negative regulators are in red, and positive regulators are in blue. **c**, Distribution of sgRNA enrichment in $FOXP3^{high}$ versus $FOXP3^{low}$ cells. sgRNA-level LFC for selected genes are indicated in red (enriched in $FOXP3^{high}$ cells) and blue (enriched in $FOXP3^{low}$ cells), whereas the overall distribution is shown in black. **d**, Gene Ontology analysis of FOXP3 negative (top) and positive (bottom) regulators. **e**,**f**, FOXP3 median fluorescence intensity (MFI) of $FOXP3^+$ cells (left) and per cent $FOXP3^+$ cells (right) after iT_{reg} induction as measured by flow cytometry of top negative (**e**) and positive (**f**) regulators. Each data point is representative of an independent biological donor ($n = 5$ donors and 4 donors, respectively). Data are presented as mean ± s.e.m. **g**, Representative histograms showing FOXP3 expression in iT_{reg} cells with indicated genetic perturbations related to the experiment in **e**,**f**. Negative (red) and positive (blue) regulators are overlaid on NTC (grey).

based on single guide RNA (sgRNA) lentiviral infection with Cas9 protein electroporation (SLICE) pooled CRISPR screens to efficiently deliver individual sgRNAs and Cas9 protein into single cells. We further extended the method by integrating phenotypic readouts via detection of intracellular transcription factor protein expression[10]. We designed a genome-wide lentiviral sgRNA library based on optimized sgRNA sequences from the Brunello library to transduce human naive $CD4^+$ T cells[15]. We then electroporated cells with Cas9 protein to mediate specific perturbation of targeted genes and expanded the cells before induction of FOXP3 expression through TCR activation and the addition of exogenous TGFβ and IL-2 (Extended Data Fig. 1a). We collected and stained the cells for FOXP3 protein 72 h after iT_{reg} induction and

then sorted on the basis of endogenous FOXP3 protein expression by categorically binning the cells into FOXP3^{low} and FOXP3^{high} populations (Fig. 1a and Extended Data Fig. 1b).

We used model-based analysis of genome-wide CRISPR–Cas9 knockout (MAGeCK)[16] to computationally identify sgRNA enrichment between FOXP3^{low} and FOXP3^{high} bins (Supplementary Table 1). Top positive and negative regulators from the screen were highly consistent between both replicates of the screen, indicating a robust screening protocol (Extended Data Fig. 1c). Our screen revealed many well-known regulators of iT$_{reg}$ FOXP3 induction including *TGFBR1*, *SMAD3/4*, *UHRF1* and *FOXP3* itself[4,17–19], but also identified novel positive and negative regulators such as *SMARCB1*, *MIDN* and *SIK3* (Fig. 1b,c). Our approach contrasts with previous efforts in mice, which only focused on the maintenance and stability of FOXP3 expression through perturbations in nT$_{reg}$ cells[12,13] (Extended Data Fig. 1d). Gene Ontology analysis of negative FOXP3 regulators uncovered a notable enrichment for members involved in Notch intracellular domain transcriptional regulation, including *RBPJ*, *HDAC3*, *GPS2*, *TBL1XR1* and *NCOR1/2*, but was also enriched for pathways involving T cell activation and ubiquitin E3 ligase (Fig. 1d). Among positive regulators of FOXP3, we observed enrichment for genes involved in transcription initiation, chromatin organization, histone modifications and protein glycosylation (Fig. 1d).

We next sought to validate the top hits from our screen through individual knockouts in an arrayed format with Cas9–gRNA ribonucleoprotein (RNP). For these experiments, we used Cas9 protein complexed with two different gRNAs against the same target to maximize knockout efficiency[20] (Extended Data Fig. 1e). Although some donor-dependent effects were evident, the observed trend was generally consistent with the results obtained from our screen (Fig. 1e–g and Extended Data Fig. 1f). Moreover, we were able to uncouple FOXP3 expression (median fluorescence intensity) and iT$_{reg}$ induction efficiency (percent FOXP3-expressing cells) by identifying cases in which the two diverged (*DNMT1* and *CUL3*) or moved synergistically (*RBPJ* and *SIK3*). Similarly, for FOXP3 positive regulators, *DHX36* depletion decreased FOXP3 protein expression despite a similar iT$_{reg}$ induction rate, perhaps reflective of the post-transcriptional regulatory function of *DHX36* in mediating translational output[21] (Fig. 1g). Together, our genome-wide screen highlights the apparent diversity of molecular mechanisms involved in *FOXP3* regulation.

Perturbation analysis with icCITE-seq

To unbiasedly assess global transcriptomic and select protein changes resulting from the perturbation of each putative FOXP3 regulator, we coupled pooled CRISPR knockouts with single-cell RNA readouts and protein detection with intracellular CITE-seq (Perturb-icCITE-seq). Because standard single-cell RNA platforms fail to faithfully capture *FOXP3* mRNA expression[22,23], we leveraged icCITE-seq to validate candidate regulators nominated from our whole-genome screen by quantifying FOXP3 protein expression at single-cell resolution[24].

We performed Perturb-icCITE-seq in human primary T cells undergoing iT$_{reg}$ polarization, targeting 296 candidate hits and controls from our genome-wide screen while simultaneously profiling over 300 different surface and intracellular epitopes (Fig. 2a). Reassuringly, targeted knockout of *FOXP3* was followed by a concomitant decrease in signal for intracellular FOXP3 protein, whereas targeting *RBPJ*, *SIK3* and *ZBTB7B* increased it (Fig. 2b). These trends were also apparent for other targeted genes such as *IKZF3*, *LCP2* (which encodes SLP76) and *MAPK1* (which encodes ERK2; Fig. 2b and Extended Data Fig. 2a), validating the epitope-specific profiling for these intracellular proteins. Similarly, we uncovered dynamic regulation between targeted knockouts and the expression of specific surface epitopes (Extended Data Fig. 2b and Supplementary Table 2). For example, perturbation of *STAT5B*, a known regulator of CD25 expression[25], sharply decreased surface CD25 protein expression levels, whereas expression was increased in *STK11*-knockout cells (Fig. 2b).

Globally, quantifying FOXP3 protein levels enabled robust validation of 91 putative regulators from our genome-wide screen (Extended Data Fig. 2c). Moreover, we observed high concordance between FOXP3 protein expression in target knockouts and their respective gRNA enrichment from the CRISPR screen ($r = -0.71$; Fig. 2c). Of note, *ZBTB7B* and intracellular Notch signalling effectors (*RBPJ*, *HDAC3* and *GPS2*) emerged as top negative regulators, exhibiting increased expression of FOXP3 protein upon perturbation (Extended Data Fig. 2c). Conversely, genes such as *CBFB*, *SMARCB1*, *MIDN* and *DAD1* were identified as top positive regulators. These findings underscore the utility of Perturb-icCITE-seq for quantitative assessments of perturbation-induced changes in surface and intracellular protein expression.

Co-functional modules and gene programs

We next sought to model the effects of genetic perturbations of individual genes on transcriptomic profiles by applying the MIMOSCA framework[26,27] (Supplementary Methods). The resulting regulatory model associated 227 targeted knockout genes to 2,192 significantly changed genes, which could be further clustered into 11 co-functional target gene modules (perturbation target modules A–K) and 10 gene-co-regulated programs (GP1–10; Fig. 2d, Extended Data Fig. 2d–f and Supplementary Table 3). The learned model correctly inferred the effect of genes known to affect the TCR (*CD3D*, *CD3E* and *LCP2*) and TGFβ (*SMAD3*, *SMAD4*, *TGFBR1* and *TGFBR2*) signalling pathways and partitioned these genes into discrete target gene modules (module F and module J, respectively; Extended Data Fig. 2g).

The parsing of individual gene programs contextualized the regulatory interplay between target genes and specific cellular processes such as the T cell effector response (GP3 and GP10), chromatin regulation (GP1), IL-2 signalling (GP5) and cellular metabolism (GP6, GP7 and GP8; Fig. 2e). For example, perturbation of module K (encompassing genes such as *PGM3* and *GFPT1*) resulted in a metabolic shift towards aerobic glycolysis (GP7) with a decrease in IL-2 signalling (GP5), oxidative phosphorylation (GP6) and *FOXP3* expression, which is consistent with their known regulatory roles on the hexosamine biosynthetic pathway and its effects on T helper 17 versus iT$_{reg}$ balance[28]. Upon closer examination, we observed that module K also had additional members from the downstream N-linked protein glycosylation pathway: namely, *ALG2*, *RPN1*, *DAD1* and *ALG11*. These perturbations exhibited a strong resemblance to the effects seen in *PGM3* and *GFPT1* and, notably, have not been previously implicated in *FOXP3* expression (Extended Data Fig. 3a,b). In target gene module G, membership was solely defined by the gene *ZBTB7B* (also known as *ThPOK*), which showed a strong enrichment for T cell effector responses (GP10), cytoskeleton remodelling (GP8), active translation (GP9) and IL-2 signalling (GP5; Fig. 2e). Inspection of affected genes revealed the activation of a cytotoxic CD8$^+$ T cell gene program[29,30], consisting of pronounced expression of *CD8A*, *XCL1/2*, *CTSW*, *GZMB*, *NKG7* and *RUNX3*, and downregulation of *CD4*, despite increased *FOXP3* expression (Fig. 2b and Extended Data Fig. 3c).

In module I, membership exclusively comprised genes linked with the NCOR transcriptional repressor complex (*GPS2*, *HDAC3*, *NCOR1* and *TBL1XR1*), which were identified as negative regulators of *FOXP3* expression in our initial genome-wide screen[31] (Fig. 1b,e). Despite its known interaction with the complex, *RBPJ*[32] was surprisingly missing from this module and was instead associated with module H. A comparative analysis of the regulatory profiles of these factors revealed that *RBPJ* ablation induces a somewhat distinct transcriptional signature compared with the other constituents of the NCOR complex (Extended Data Fig. 3d). Given the established interactions of NCOR with various other transcription factors such as BCL6, Kaiso, ETO, MEF2C and CBF1 (ref. 31), these results probably indicate that *RBPJ* accounts for only a subset of NCOR-repressive function.

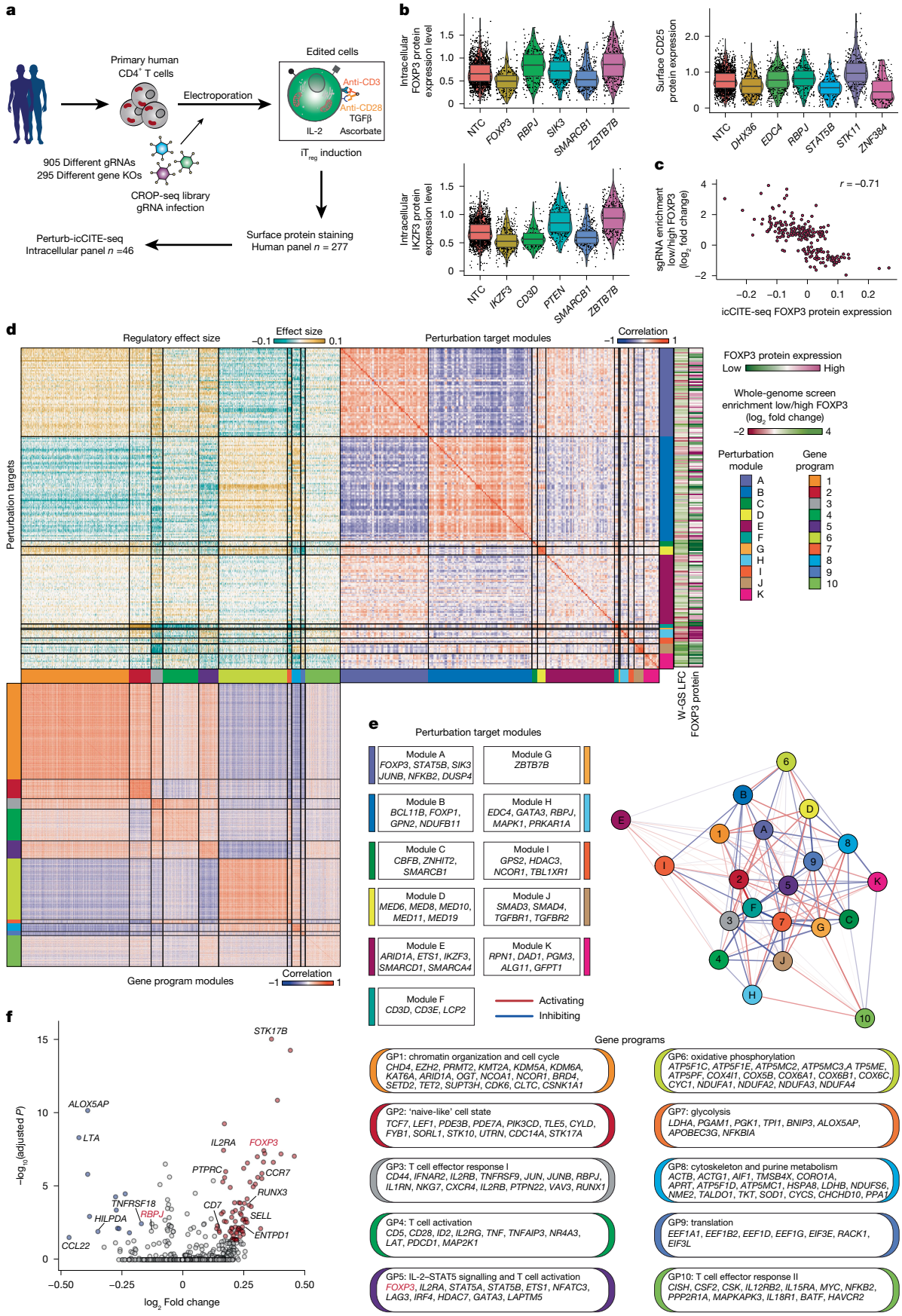

Fig. 2 | See next page for caption.

Fig. 2 | Validation of *FOXP3* regulators with Perturb-icCITE-seq. a, Schematic of pooled CRISPR screens in human iT_{reg} cells with Perturb-icCITE-seq. Adapted from ref. 51, Springer Nature America, Inc. KO, knockout. **b**, Violin plots for the indicated proteins showing the distribution of protein counts for select targeted genes (KO). The boxplot spans from the first to the third quartile of the distribution, with the median positioned in the centre. Whiskers represent the minimum and maximum values, excluding outliers. Values plotted represent cells from a single replicate. **c**, Scatterplot of FOXP3 protein expression score (Methods) associated with each perturbed target plotted against its gene-level LFC enrichment in $FOXP3^{low}$ versus $FOXP3^{high}$ cells derived from the whole-genome CRISPR screen (Supplementary Table 1). **d**, Co-functional target modules and gene-co-regulated programs from the Perturb-icCITE-seq screen. A β-regulatory matrix with regulatory effect sizes for perturbation (KO) of each targeted gene (rows) on expression of 2,192 affected genes (columns; top left). Pearson correlation coefficient of perturbed genes (top right). FOXP3 protein expression score and whole-genome CRISPR screen (W-GS) LFC enrichment for each targeted gene are indicated on the right. Pearson correlation coefficient of significantly affected gene features (bottom left) is also shown. **e**, Regulatory network depicting mean effects of co-functional target modules on each gene-co-regulated program. Positive (activating) effects are indicated in red, whereas negative (inhibiting) effects are highlighted in blue. **f**, Volcano plot of differentially regulated genes between FOXP3-expressing *RBPJ*-knockout and control-edited iT_{reg} cells as determined by Perturb-icCITE-seq. The *x* axis shows the LFC, and the *y* axis shows $-\log_{10}$ of the adjusted *P* value calculated using the Wilcoxon rank-sum test with Bonferroni correction for multiple testing.

We next probed potential regulatory relationships between perturbed targets by examining the transcriptional effects of the perturbed targets on each other. Unexpectedly, our analyses revealed a notable number of regulatory interactions across perturbation-targeted genes on *RBPJ*, suggesting that *RBPJ* may act as a central 'hub' in iT_{reg} cells and is tightly regulated by various signalling cues (Extended Data Fig. 3e,f).

To further understand the transcriptional effect of *RBPJ* ablation, we compared differential gene expression with non-targeting control (NTC) in *FOXP3*-expressing iT_{reg} cells (Supplementary Methods). Our analysis revealed that *RBPJ*-knockout iT_{reg} cells expressed higher levels of core effector genes of T_{reg} function such as *FOXP3*, *IL2RA* and *ENTPD1* (Fig. 2f). Moreover, a similar analysis conducted on differential protein expression uncovered higher expression of CD39, Tim-3 and CTLA4, indicating that *RBPJ* knockout may augment iT_{reg}-suppressive activity (Extended Data Fig. 3g). Together, these data highlight the power of Perturb-icCITE-seq for scalable, systematic validation of large-scale CRISPR screens targeting intracellular proteins, thereby identifying *RBPJ* as a novel repressor of *FOXP3* expression.

RBPJ is a negative regulator of FOXP3

As our single-cell analyses and subsequent validation experiments identified RBPJ as a TGFβ-dependent strong negative regulator of *FOXP3* expression in both human and mouse T cells (Fig. 2 and Extended Data Figs. 3 and 4a–g), we investigated its phenotype in more detail. RBPJ is a well-known major downstream transcriptional activator of Notch-responsive genes through its association with the Notch intracellular domain (NICD) and mastermind-like protein (MAML1–3)[33–35]. However, in the absence of active Notch signalling, RBPJ forms a co-repressor complex along with NCOR1/2 and HDAC3 to mediate transcriptional repression[32,36,37]. Although our whole-genome screen suggested significant enrichment for the RBPJ co-repressor complex, we could not exclude potential contributions of canonical Notch signalling that were missed due to the sensitivity of the screen (Fig. 3a). We therefore sought to refine our findings through genetic and pharmacological manipulations systematically targeting the Notch signalling pathway. In congruence with our initial screen, we did not find significant changes in FOXP3 protein expression in response to Notch-effector perturbations (Fig. 3b and Extended Data Fig. 4h,i). In addition, consistent with a previous report[38], we did not find any substantial effects on FOXP3 expression in *RBPJ*-depleted nT_{reg} cells (Extended Data Fig. 4j). Together, these results suggest that the *RBPJ* perturbation-induced phenotype is contextually dependent and independent of canonical Notch signalling.

Because our CRISPR validation experiments required TCR pre-stimulation, we wanted to disentangle potential confounding effects that may have arisen through multiple rounds of TCR activation. To this end, we treated freshly isolated naive $CD4^+$ T cells undergoing iT_{reg} polarization using *RBPJ*-targeting antisense oligonucleotides (ASOs). We observed a higher percentage of cells expressing FOXP3 as well as higher expression of FOXP3 in *RBPJ*-targeting ASOs than in NTCs, confirming that these effects were not dependent on TCR pre-stimulation (Fig. 3c and Extended Data Fig. 4k–m). Moreover, examination of differentially expressed genes in NTC cells versus *RBPJ*-knockout resting T cells showed no enrichment for FOXP3 regulators identified in our genome-wide screen (Extended Data Fig. 4n). Collectively, these data indicate a direct role of RBPJ in regulating FOXP3 expression.

We next sought to validate the findings of our single-cell data by comparing global gene expression between *RBPJ*-depleted and NTC iT_{reg} cells at the bulk level using RNA-seq. To mitigate potential confounding effects arising from an increased proportion of $FOXP3^+$ cells in *RBPJ*-ablated iT_{reg} cells when compared with NTC iT_{reg} cells, we developed intracellular RNA-seq (icRNA-seq), which enables the isolation of high-quality RNA from FOXP3-expressing cells by flow cytometry (Extended Data Fig. 5a–d). *RBPJ* deletion induced broad transcriptomic changes in $FOXP3^+$ iT_{reg} cells, including increased mRNA expression of *FOXP3* and decreased expression of *RBPJ* and *SGK1* (Fig. 3d,e). Overall, our bulk observations with icRNA-seq were in line with our previous single-cell analyses (Extended Data Fig. 5e). We observed increased RNA expression of core T_{reg} lineage genes such as *IL2RA* and *ENTPD1*, but also additionally identified genes such as *ICOS*, *TIGIT*, *HAVCR2* (encoding Tim-3) and *LRRC32* (Fig. 3d,e). Gene set enrichment analysis (GSEA) demonstrated the upregulation of a 'T_{reg}-like' transcriptomic signature in *RBPJ*-knockout iT_{reg} cells (Fig. 3f and Extended Data Fig. 5f), suggesting that perturbation of *RBPJ* may impart iT_{reg} cells with transcriptional characteristics that more closely resemble T_{reg} lineage identity. On the basis of these findings, we hypothesized that modulation of *RBPJ* may further enhance iT_{reg} functionality.

RBPJ ablation improves iT_{reg} function

Conserved noncoding sequence (CNS) *cis*-regulatory regions located at the *Foxp3* gene have been previously shown to have critical roles in the regulation of FOXP3 expression[39–43]. In particular, the T_{reg}-specific demethylated enhancer region CNS2 has been closely linked with the stability of FOXP3 (refs. 6,44). Although various approaches modulating TCR co-stimulation or activity of DNA methylation-related enzymes have been demonstrated to be effective in conferring T_{reg}-type CNS2 demethylation in mice, these approaches thus far have not been conducive in human iT_{reg} cells[45,46]. We thus asked whether *RBPJ*-knockout iT_{reg} cells also exhibit DNA methylation changes at CNS2. In agreement with previous studies, NTC iT_{reg} cells only displayed a modest degree of CNS2 CpG demethylation[46,47] (Fig. 3g and Extended Data Fig. 6a). Unexpectedly, we found that *RBPJ* deficiency in iT_{reg} cells was consistently followed by an increased loss of CpG methylation, which was dependent on the addition of ascorbate, indicating that the perturbed cells exhibit increased de novo CNS2 demethylation over NTCs.

Considering that CNS2 demethylation at the *FOXP3* locus safeguards the expression of FOXP3 in T_{reg} cells from inhibitory effects of pro-inflammatory signalling molecules[40], we reasoned that the increased demethylation observed in *RBPJ*-knockout iT_{reg} cells could potentially enhance resilience in FOXP3 expression against prolonged exposure to

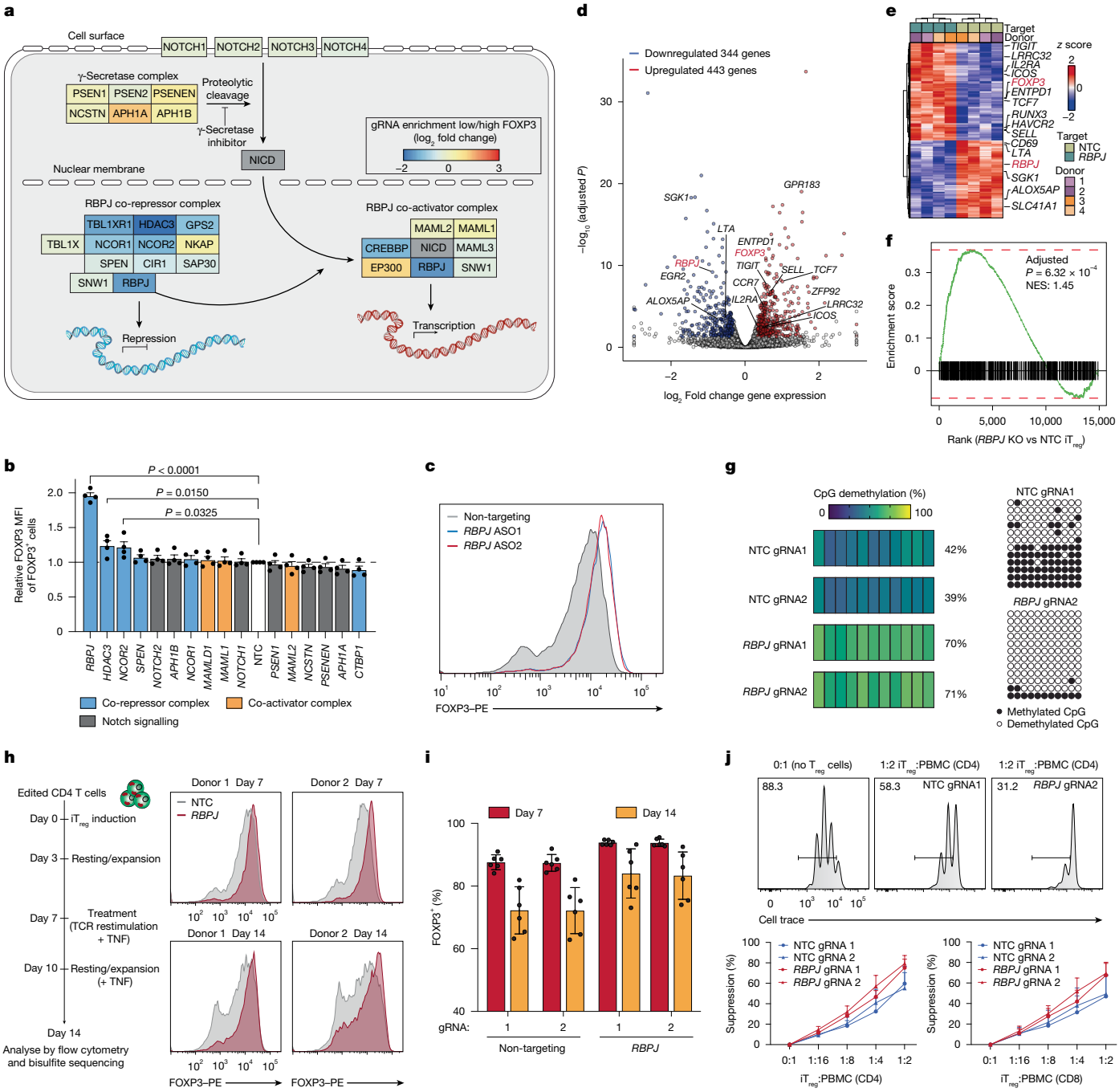

Fig. 3 | *RBPJ* knockout improves *FOXP3* expression, function and stability in iT_{reg} cells. a, Molecular map of genes with previous evidence of involvement in the Notch signalling pathway. Boxes are coloured according to the LFC score from the whole-genome CRISPR screen. **b**, Comparison of FOXP3 MFI in iT_{reg} cells with the indicated genetic perturbations ($n = 4$ donors). Data are presented as mean ± s.e.m. Statistical analysis was performed with a one-way analysis of variance (ANOVA) with Dunnett's multiple comparison test. **c**, Histogram showing FOXP3 expression in iT_{reg} cells treated with ASOs, representative of four independent donors. **d**, Volcano plot depicting differential genes between *RBPJ*-knockout and control-edited $FOXP3^+$ iT_{reg} cells as determined by icRNA-seq. The *x* axis shows the LFC, and the *y* axis shows $-\log_{10}$ of the adjusted *P* value calculated using the Wilcoxon rank-sum test with Bonferroni correction for multiple testing. **e**, Heatmap of differentially expressed genes in *RBPJ*-knockout versus NTC $FOXP3^+$ iT_{reg} cells. **f**, GSEA of differentially expressed genes between human nT_{reg} cells and T_{conv} cells. Adjusted *P* value was determined by a two-sided permutation test. **g**, Summarized DNA methylation status at each of the 11 CpGs located at the *FOXP3* CNS2 locus ($n = 4$ donors; left), and a representative plot of CNS2 DNA methylation status (right). **h**, Experimental schematic for modelling iT_{reg} stability in vitro (left), and representative histograms from two independent donors showing FOXP3 stability before and after treatment in NTC or *RBPJ*-knockout iT_{reg} cells (right). Adapted from ref. 51, Springer Nature America, Inc. **i**, Summarized data of the experiment in **h**. Stability was assessed by flow cytometry ($n = 6$ donors). Data are presented as mean ± s.e.m. **j**, Suppression assay confirms higher suppressive activity in *RBPJ*-ablated iT_{reg} cells (top). Numbers are indicative of the percentage of dividing cells. A summary of iT_{reg} in vitro suppression experiments with responder $CD4^+$ (bottom left) and $CD8^+$ (bottom right) T cells at the indicated ratios is also shown. Data are presented as mean ± s.e.m. for three independent donors. PBMC, peripheral blood mononuclear cell.

inflammatory cytokines. As expected, *RBPJ* ablation augmented lineage stability under conditions with repeated TCR stimulations and exogenous TNF, resulting in more FOXP3$^+$ iT$_{reg}$ cells (Fig. 3h,i and Extended Data Fig. 6b). Stratifying these cells based on FOXP3 expression levels revealed markedly different demethylation patterns compared with NTC cells (Extended Data Fig. 6c). In mice, Cre-induced knockout of *Rbpj* in *Rbpj*$^{flox/flox}$ conventional T (T$_{conv}$) cells similarly produced more stable iT$_{reg}$ cells that maintained higher expression levels of FOXP3, consistent with our findings in human counterparts (Extended Data Fig. 6d). Moreover, *Rbpj* deletion in FOXP3-committed iT$_{reg}$ cells also affected its regulation, resulting in a higher percentage of FOXP3-expressing T$_{reg}$ cells after prolonged culture (Extended Data Fig. 6e). Together, these results provide evidence for a role of RBPJ in FOXP3 stability and maintenance.

Given the increased expression and stability of FOXP3, as well as the heightened expression of functional effector genes such as those encoding CTLA4 and CD25 in *RBPJ*-knockout iT$_{reg}$ cells (Fig. 2f and Extended Data Figs. 3g and 6f,g), we hypothesized that these cells may exhibit increased suppressive function. Indeed, *RBPJ*-ablated iT$_{reg}$ cells were more potent to suppress CD4$^+$ and CD8$^+$ T effector cells than NTC cells, indicating higher in vitro suppressive activity (Fig. 3j). Collectively, these data strongly support the notion that *RBPJ*-ablated iT$_{reg}$ cells exhibit heightened differentiation, stability and functionality in vitro.

RBPJ regulates *FOXP3* through NCOR

To identify critical domains of RBPJ required for the repression of *FOXP3*, we performed high-density mutagenesis using 151 different sgRNAs targeting exon-coding regions of the *RBPJ* locus. In this experimental system, increased sgRNA enrichment in FOXP3^{high} cells can also be indicative of an increased likelihood of in-frame mutations occurring in functional residues, leading to a loss-of-function outcome[48]. We observed increased enrichment scores especially when targeting sequences coding for the β-trefoil DNA-binding domain and the C-terminal domain, both of which have been demonstrated to be critical in mediating the interface between RBPJ and the SMRT–NCOR repressive complex[49] (Fig. 4a, Extended Data Fig. 7a and Supplementary Table 4). Consistent with the dependence on these domains, the SMRT–NCOR-interacting defective RBPJ mutant F235A/L362A (hereafter referred to as mutant RBPJ) largely rescued the profound FOXP3 induction defect observed in RBPJ-transduced CD4$^+$ T cells undergoing iT$_{reg}$ polarization (Fig. 4b). In line with our previous observations on context dependency, ectopic expression of RBPJ in committed iT$_{reg}$ cells strongly suppressed FOXP3 expression but was only marginally affected in nT$_{reg}$ cells (Extended Data Fig. 7b,c).

We hypothesized that RBPJ may mediate its effects through direct regulation of the *FOXP3* locus during iT$_{reg}$ differentiation. We therefore evaluated RBPJ binding to the *FOXP3* transcription start site (TSS) using an electrophoretic mobility shift assay (EMSA) with DNA probes spanning the RBPJ consensus motif TTTCCCAC and nuclear extracts from human CD4$^+$ T cells undergoing iT$_{reg}$ polarization. EMSA revealed RBPJ binding directly at the *FOXP3* promoter of these cells, which is supportive of the notion of direct transcriptional regulation (Extended Data Fig. 7d). To assess the functional relevance of this binding, we cloned the *FOXP3* promoter region for a luciferase assay and assessed promoter activity in iT$_{reg}$ cells. We found a strong increase in luciferase expression upon disruption of the RBPJ consensus motif and a decrease in basal expression levels upon RBPJ overexpression, consistent with our previous results (Fig. 4c).

Although our efforts delineated the effects of *RBPJ* ablation in *FOXP3* regulation, our whole-genome screen and validation experiments implicated the coordinated involvement of the NCOR repressive complex centred around RBPJ. Moreover, our RBPJ transduction experiments suggested that this physical interaction was essential for mediating RBPJ-dependent *FOXP3* repression (Fig. 4b). We therefore concentrated our subsequent efforts towards characterizing the mechanistic role of this complex. Specifically, we focused on the role of HDAC3, the core catalytic component of the NCOR co-repressor[50] and a top hit in our whole-genome screen and validation experiments (Extended Data Fig. 7e). As expected, interaction-deficient mutant RBPJ abolished the ability of RBPJ to interact with HDAC3 (Fig. 4d). To further explore the importance of this interaction, we generated *HDAC3* knockouts and observed that these cells rescued iT$_{reg}$ differentiation defects resulting from RBPJ overexpression with negligible effects in mutant RBPJ-transduced cells (Fig. 4e). Together, our results substantiate the direct involvement of HDAC3 in *FOXP3* regulation through its interaction with RBPJ.

Histone deacetylation by RBPJ–HDAC3

Given the histone deacetylation function of HDAC3 and its well-established role in gene repression, we investigated whether loss of RBPJ could alter local histone acetylation levels at the *FOXP3* locus. To this end, we conducted chromatin immunoprecipitation followed by sequencing (ChIP–seq) analyses on H3ac, H3K9ac and H3K27ac in *RBPJ*-deficient and NTC iT$_{reg}$ cells. In line with the observed higher FOXP3 expression in *RBPJ*-deficient iT$_{reg}$ cells, we found that these cells also displayed increased H3ac and H3K9ac levels across the *FOXP3* locus, implicating a potential role for RBPJ in regulating these histone modifications through recruitment of HDAC3 (Fig. 4f and Extended Data Fig. 7f). Of note, this trend was not observed for H3K27ac, indicating that this finding was not merely a consequence of an increased proportion of FOXP3$^+$ cells (Extended Data Fig. 7g).

We next wanted to contextualize the relevance of histone acetylation in FOXP3 regulation, given our previous results that indicated the involvement of HDAC3 through its association with RBPJ. We hypothesized that a local loss in histone acetylation through modulation by HDAC3 at *FOXP3* underlay the decrease in iT$_{reg}$ induction efficiency and FOXP3 expression in cells transduced with RBPJ. However, we wanted to also avoid potential confounding effects on histone acetylation resulting from a decreased proportion of FOXP3$^+$ iT$_{reg}$ cells in RBPJ-overexpressed cells. To overcome these technical constraints, we developed intracellular ChIP–seq (inChIP–seq) and intracellular ATAC-seq (inATAC-seq) by modifying our previous ASAP-seq[51] intracellular staining protocol to specifically enrich for the FOXP3-expressing fraction of cells by flow cytometry before downstream processing with ChIP–seq or ATAC-seq, respectively (Extended Data Fig. 8a–c). Accordingly, inChIP–seq of FOXP3$^+$ cells from RBPJ-transduced iT$_{reg}$ cells revealed decreased H3K9ac and total H3ac levels at the *FOXP3* locus compared with mock-transduced controls (Fig. 4g). This was further complemented with a similar decrease in accessible chromatin, which spanned the *FOXP3* TSS and CNS2. By contrast, mutant RBPJ-transduced cells did not exhibit substantial changes in local H3ac or H3K9ac, which is consistent with its inability to associate with HDAC3 (Extended Data Fig. 8d).

To further corroborate our findings, we generated high-resolution profiles of RBPJ binding at the *FOXP3* locus using CUT&RUN on RBPJ-transduced cells undergoing iT$_{reg}$ differentiation[52–54]. We used an AM tag-specific antibody to probe for epitope-tagged RBPJ, which revealed enrichment for RBPJ chromatin occupancy at the *FOXP3* TSS, CNS1 and CNS0 (Fig. 4g). Reassuringly, a similar binding pattern was also observed for mutant RBPJ, which indicated that rescue of FOXP3 expression was not an artefact of compromised DNA-binding ability of the mutant to the *FOXP3* TSS. We found that mutant RBPJ did not bind to the TGFβ-responsive enhancer CNS1 (ref. 39), suggesting that RBPJ binding through CNS1 may also account for its ability to negatively regulate FOXP3 induction and expression. Together, our results strongly support the notion that engagement of RBPJ with the NCOR complex directly represses FOXP3 expression through modulation of histone acetylation.

RBPJ knockout improves iT$_{reg}$ function in vivo

To assess the translational applicability of these findings, we tested whether *RBPJ*-deficient iT$_{reg}$ cells would display enhanced functionality

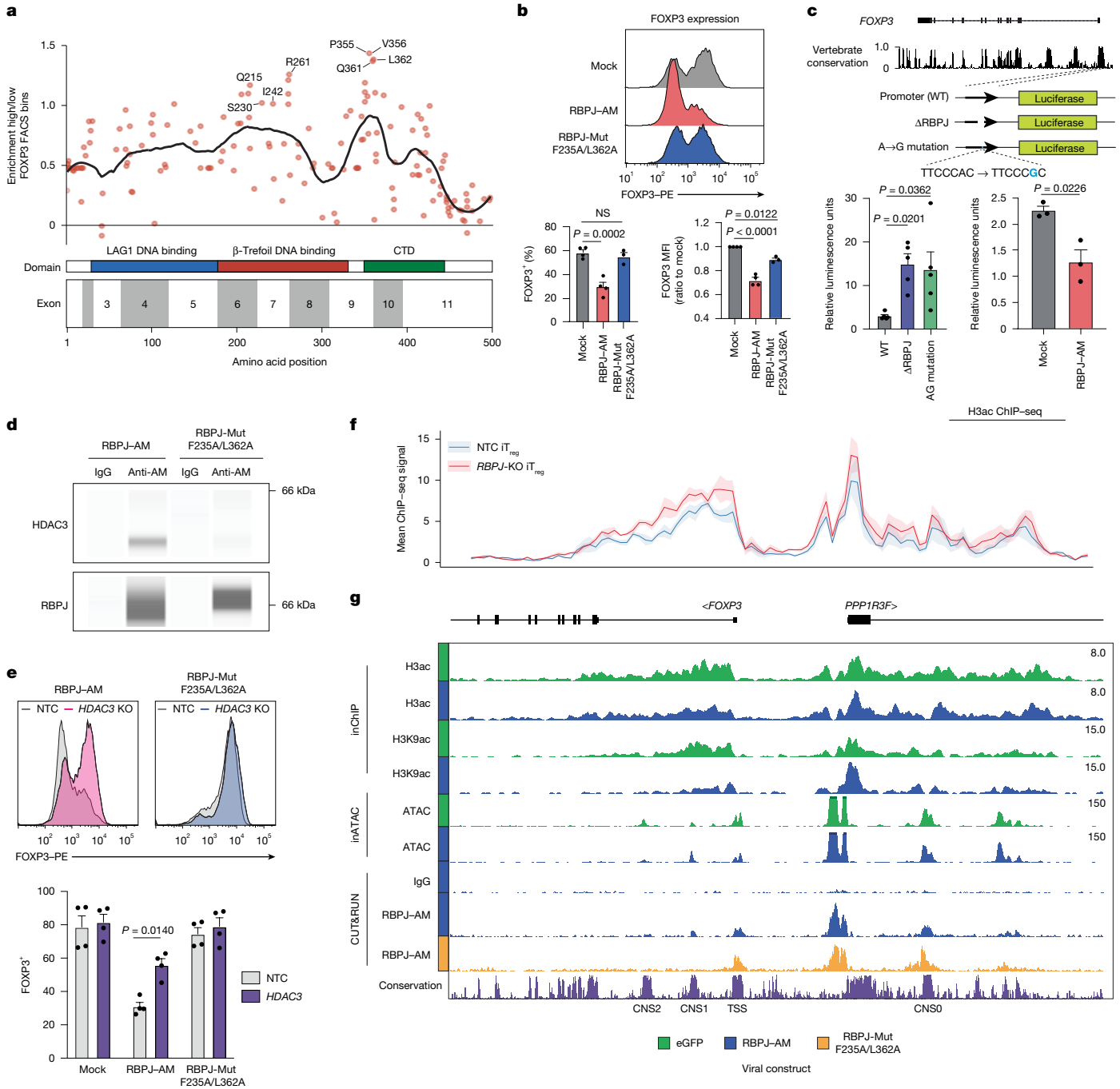

Fig. 4 | The RBPJ–NCOR–HDAC3 complex directly represses FOXP3 through modulation of local histone acetylation. a, Saturation mutagenesis of the *RBPJ* coding sequence by pooled CRISPR screening. Each circle represents the enrichment score for an individual sgRNA across three independent donors. The black line is the locally estimated scatterplot smoothing curve. **b**, RBPJ-transduced or RBPJ-mutant-overexpressing lentivirus-transduced human CD4$^+$ T cells were polarized into iT$_{reg}$ cells ($n = 4$ donors; 3 donors for RBPJ-Mut), assessed for FOXP3 expression (top) and quantified for per cent FOXP3$^+$ and MFI (bottom). **c**, Human CD4$^+$ T cells were nucleofected with luciferase reporter constructs containing the *FOXP3* promoter reference sequence (WT), RBPJ-binding site mutated (A→G mutation) or RBPJ-binding site deleted (ΔRBPJ) *FOXP3* promoter sequences and assessed for luciferase activity under FOXP3-inducing conditions ($n = 5$ donors; bottom left). RBPJ-transduced or mock-transduced cells were electroporated with a WT *FOXP3* promoter luciferase reporter construct and cultured under FOXP3-inducing conditions before measuring luciferase activity ($n = 3$ donors; bottom right). **d**, Co-immunoprecipitation analysis of the interaction between RBPJ or F235A/L362A RBPJ-Mut and HDAC3 in human iT$_{reg}$ cells. **e**, Histogram of FOXP3 expression in *HDAC3*-deleted or control iT$_{reg}$ cells transduced with RBPJ (top left) or F235A/L362A-mutant RBPJ (top right). Summarized data of the experiment across four independent donors (bottom) are also shown. **f**, Summary of H3ac ChIP–seq signal enrichment at *FOXP3*. Data are plotted as mean ± s.e.m. for three independent donors. **g**, H3ac and H3K9ac inChIP–seq, inATAC-seq, CUT&RUN (control IgG and anti-AM antibody) and PhastCons species conservation tracks in iT$_{reg}$ cells. All data are presented as mean ± s.e.m. NS, not significant. Statistical analysis was performed with a one-way ANOVA with Dunnett's multiple comparison test for **b**,**c** (bottom left), two-tailed paired Student's *t*-test for **c** (bottom right) and **e** (bottom). Data are representative of four independent donors in **b** (top) and **e** (top), and two to three independent donors for **g**.

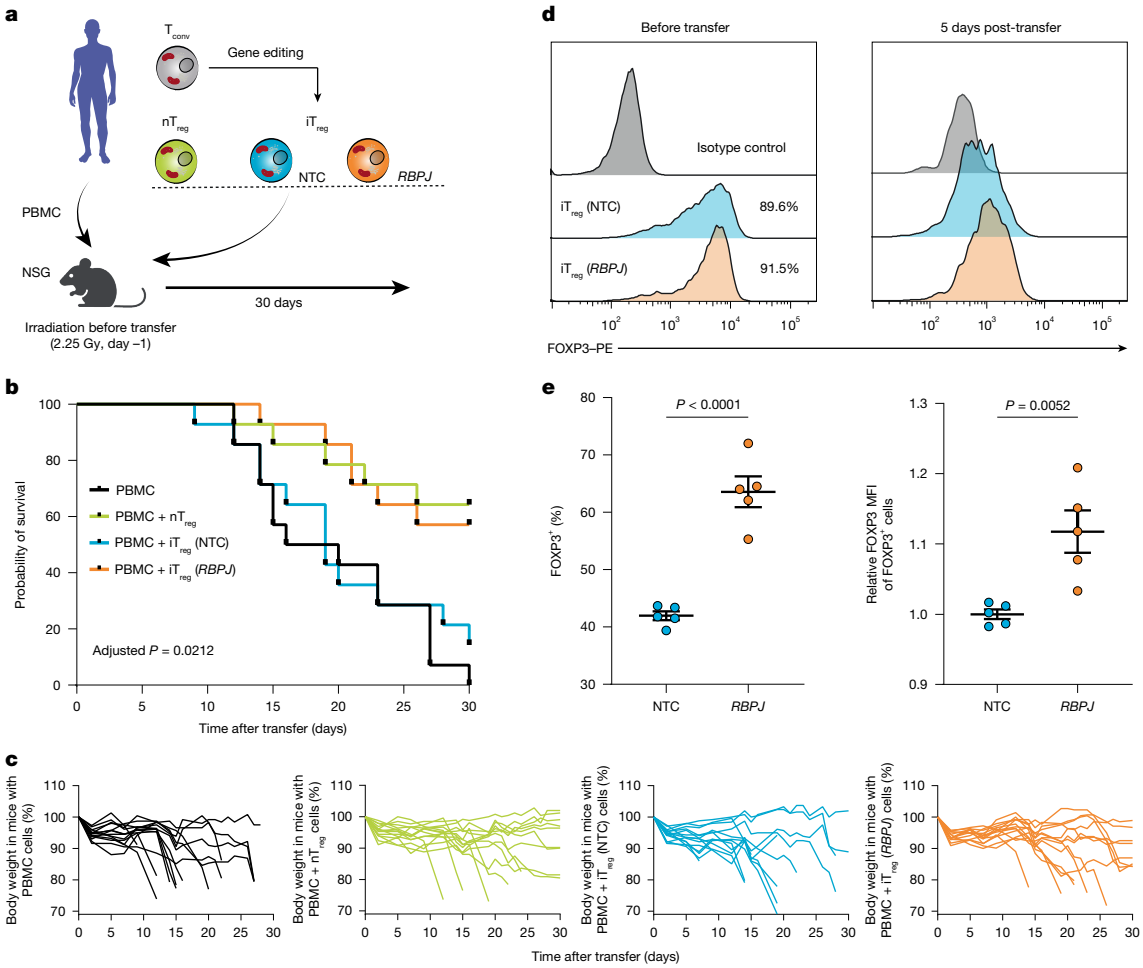

Fig. 5 | *RBPJ* ablation improves iT_{reg} in vivo stability and suppressive function. **a**, Schematic depicting the xenogeneic GvHD model used to evaluate *RBPJ*-knockout iT_{reg} function in vivo (Methods). The silhouettes of the human and mouse were created using BioRender (https://biorender.com), and the rest of the schematic was adapted from ref. 51, Springer Nature America, Inc. **b**, Survival curve for the indicated conditions ($n = 14$). Survival P values by log-rank test were adjusted for multiple testing. **c**, Relative body weight change of the cohort in **b** over time. **d**, Histogram of FOXP3 expression before (left) and after (right) transfer. The isotype control is indicated in grey. **e**, Statistical analysis of the per cent of FOXP3 and FOXP3 MFI in iT_{reg} cells 5 days post-transfer ($n = 5$), related to the data presented in **d**. Data are presented as mean ± s.e.m. Statistical analysis was performed with a two-tailed unpaired Student's t-test.

in vivo and improve performance in a xenogeneic GvHD model (Fig. 5a). In this model, mice that received NTC iT_{reg} cells were not protected from GvHD-induced lethality. By contrast, mice receiving nT_{reg} or *RBPJ*-deficient iT_{reg} cells showed substantial improvements, with iT_{reg} cells showing similar potency to nT_{reg} cells (Fig. 5b,c and Extended Data Fig. 9a,b). Similarly, *RBPJ*-knockout iT_{reg} cells exhibited sustained FOXP3 expression stability in vivo (Fig. 5d,e and Extended Data Fig. 9c), consistent with our in vitro observations (Fig. 3). In summary, these data demonstrate that *RBPJ* ablation can potently augment the efficacy of iT_{reg}-mediated suppression in vivo, highlighting its modulation as a novel target in iT_{reg}-based therapeutics.

Discussion

The stability and efficacy of iT_{reg} cells are two major challenges for adoptive cell transfer therapies. Here we applied genome-wide CRISPR screening to reveal genetic perturbations that positively or negatively affect FOXP3 induction and validated our results with intracellular protein staining using Perturb-icCITE-seq. Unexpectedly, we found the pronounced enrichment for RBPJ as a novel negative regulator of iT_{reg} differentiation and FOXP3 expression with minimal effects in nT_{reg} cells, highlighting the dependence on contextual cues and diverse avenues of *FOXP3* gene regulation. Of note, *RBPJ* knockout conferred enhanced stability and suppressive activity in iT_{reg} cells in vitro and in vivo. This finding stemmed from heightened FOXP3 expression with increased histone acetylation and DNA demethylation at the *FOXP3* CNS2 locus, as well as increased expression of CTLA4 and CD25. Our results therefore add to the growing interest in manipulating RBPJ for cellular therapy[55].

Mechanistically, we found that RBPJ represses FOXP3 expression through direct binding at the *FOXP3* TSS and CNS1 enhancer region, resulting in local chromatin repression through histone deacetylation. Of note, this process was dependent on recruitment of NCOR and HDAC3 by RBPJ and overexpression of an interaction-deficient mutant abolished the FOXP3-repressive ability of RBPJ. Our results therefore propose a model in which RBPJ works in concert with the NCOR repressor complex to orchestrate regulation of FOXP3 expression through *cis*-epigenetic remodelling.

Although a previous study concluded that *Rbpj*-knockout mouse $CD4^+$ T cells negatively affect iT_{reg} differentiation and FOXP3 expression[56], our results in both mice and human cells demonstrate a robust increase. One possibility for this disparity observed in earlier studies using the CD4–Cre–loxP system is that gene knockout can occur during the DP stage of developing thymocytes, potentially resulting in unintended knockout effects. Indeed, our data suggest that Cre induction in $Rbpj^{flox/flox}$ mature $CD4^+$ T cells or a similar knockout system using CRISPR–Cas9 leads to a robust increased capacity for iT_{reg} differentiation and FOXP3

expression (Extended Data Fig. 4a–g). Our results therefore underscore the wide-range function of RBPJ in governing T cell differentiation under different contexts.

To objectively compare molecular phenotypes of control and perturbed cells expressing FOXP3, we developed three novel assays, icRNA-seq, inChIP–seq and inATAC-seq, which enable the isolation of cells based on the abundance of intracellular proteins for downstream profiling by RNA-seq, ChIP–seq and ATAC-seq, respectively. Although similar methods have been previously published for ATAC-seq[57,58], our fixation and permeabilization protocol for inChIP and inATAC is uniquely compatible with downstream ChIP–seq and droplet-based single-cell ATAC experiments, allowing for the profiling of the same pool of cells using multiple assays. We envision that these methods will be widely applicable to the scientific community and particularly useful for researchers looking to quantify specific cellular populations that are classically defined by intracellular proteins.

Overall, our findings demonstrate that *RBPJ* deletion enhances the conversion, functionality and stability of iT$_{reg}$ cells, critical domains for adoptive cell transfer therapies that have, until now, posed substantial clinical challenges.

Online content

Any methods, additional references, Nature Portfolio reporting summaries, source data, extended data, supplementary information, acknowledgements, peer review information; details of author contributions and competing interests; and statements of data and code availability are available at https://doi.org/10.1038/s41586-025-08795-5.

1. Sakaguchi, S. et al. Regulatory T cells and human disease. *Annu. Rev. Immunol.* **38**, 541–566 (2020).
2. Raffin, C., Vo, L. T. & Bluestone, J. A. T$_{reg}$ cell-based therapies: challenges and perspectives. *Nat. Rev. Immunol.* **20**, 158–172 (2020).
3. Sakaguchi, S. Taking regulatory T cells into medicine. *J. Exp. Med.* **218**, e20210831 (2021).
4. Chen, W. et al. Conversion of peripheral CD4$^+$CD25$^-$ naive T cells to CD4$^+$CD25$^+$ regulatory T cells by TGF-β induction of transcription factor Foxp3. *J. Exp. Med.* **198**, 1875–1886 (2003).
5. Kanamori, M., Nakatsukasa, H., Okada, M., Lu, Q. & Yoshimura, A. Induced regulatory T cells: their development, stability, and applications. *Trends Immunol.* **37**, 803–811 (2016).
6. Floess, S. et al. Epigenetic control of the Foxp3 locus in regulatory T cells. *PLoS Biol.* **5**, e38 (2007).
7. Ferreira, L. M. R., Muller, Y. D., Bluestone, J. A. & Tang, Q. Next-generation regulatory T cell therapy. *Nat. Rev. Drug Discov.* **18**, 749–769 (2019).
8. Mikami, N., Kawakami, R. & Sakaguchi, S. New T$_{reg}$ cell-based therapies of autoimmune diseases: towards antigen-specific immune suppression. *Curr. Opin. Immunol.* **67**, 36–41 (2020).
9. Wei, J. et al. Targeting REGNASE-1 programs long-lived effector T cells for cancer therapy. *Nature* **576**, 471–476 (2019).
10. Shifrut, E. et al. Genome-wide CRISPR screens in primary human T cells reveal key regulators of immune function. *Cell* https://doi.org/10.1016/j.cell.2018.10.024 (2018).
11. Dong, M. B. et al. Systematic immunotherapy target discovery using genome-scale in vivo CRISPR screens in CD8 T cells. *Cell* **178**, 1189–1204.e23 (2019).
12. Cortez, J. T. et al. CRISPR screen in regulatory T cells reveals modulators of Foxp3. *Nature* **582**, 416–420 (2020).
13. Loo, C.-S. et al. A genome-wide CRISPR screen reveals a role for the non-canonical nucleosome-remodeling BAF complex in Foxp3 expression and regulatory T cell function. *Immunity* **53**, 143–157.e8 (2020).
14. Schumann, K. et al. Functional CRISPR dissection of gene networks controlling human regulatory T cell identity. *Nat. Immunol.* **21**, 1456–1466 (2020).
15. Doench, J. G. et al. Optimized sgRNA design to maximize activity and minimize off-target effects of CRISPR-Cas9. *Nat. Biotechnol.* **34**, 184–191 (2016).
16. Li, W. et al. MAGeCK enables robust identification of essential genes from genome-scale CRISPR/Cas9 knockout screens. *Genome Biol.* **15**, 554 (2014).
17. Tone, Y. et al. Smad3 and NFAT cooperate to induce Foxp3 expression through its enhancer. *Nat. Immunol.* **9**, 194–202 (2007).
18. Sun, X., Cui, Y., Feng, H., Liu, H. & Liu, X. TGF-β signaling controls Foxp3 methylation and T$_{reg}$ cell differentiation by modulating Uhrf1 activity. *J. Exp. Med.* **216**, 2819–2837 (2019).
19. Hori, S., Nomura, T. & Sakaguchi, S. Control of regulatory T cell development by the transcription factor Foxp3. *Science* **299**, 1057–1061 (2003).
20. Seki, A. & Rutz, S. Optimized RNP transfection for highly efficient CRISPR/Cas9-mediated gene knockout in primary T cells. *J. Exp. Med.* **215**, 985–997 (2018).
21. Sauer, M. et al. DHX36 prevents the accumulation of translationally inactive mRNAs with G4-structures in untranslated regions. *Nat. Commun.* **10**, 2421 (2019).
22. Zemmour, D. et al. Single-cell gene expression reveals a landscape of regulatory T cell phenotypes shaped by the TCR. *Nat. Immunol.* **19**, 291–301 (2018).
23. Luo, Y. et al. Single-cell transcriptomic analysis reveals disparate effector differentiation pathways in human T$_{reg}$ compartment. *Nat. Commun.* https://doi.org/10.1038/s41467-021-24213-6 (2021).
24. Chen, K. Y. et al. Joint single-cell measurements of surface proteins, intracellular proteins and gene expression with icCITE-seq. Preprint at *bioRxiv* https://doi.org/10.1101/2025.01.11.632564 (2025).
25. Freimer, J. W. et al. Systematic discovery and perturbation of regulatory genes in human T cells reveals the architecture of immune networks. *Nat. Genet.* **54**, 1133–1144 (2022).
26. Dixit, A. et al. Perturb-seq: dissecting molecular circuits with scalable single-cell RNA profiling of pooled genetic screens. *Cell* **167**, 1853–1866.e17 (2016).
27. Frangieh, C. J. et al. Multimodal pooled Perturb-CITE-seq screens in patient models define mechanisms of cancer immune evasion. *Nat. Genet.* **53**, 332–341 (2021).
28. Araujo, L., Khim, P., Mkhikian, H., Mortales, C.-L. & Demetriou, M. Glycolysis and glutaminolysis cooperatively control T cell function by limiting metabolite supply to N-glycosylation. *eLife* **6**, e21330 (2017).
29. Setoguchi, R. et al. Repression of the transcription factor Th-POK by Runx complexes in cytotoxic T cell development. *Science* **319**, 822–825 (2008).
30. Wang, L. et al. The zinc finger transcription factor Zbtb7b represses CD8-lineage gene expression in peripheral CD4$^+$ T cells. *Immunity* **29**, 876–887 (2008).
31. Oberoi, J. et al. Structural basis for the assembly of the SMRT/NCoR core transcriptional repression machinery. *Nat. Struct. Mol. Biol.* **18**, 177–184 (2011).
32. Kao, H. Y. et al. A histone deacetylase corepressor complex regulates the Notch signal transduction pathway. *Genes Dev.* **12**, 2269–2277 (1998).
33. Fortini, M. E. & Artavanis-Tsakonas, S. The suppressor of hairless protein participates in Notch receptor signaling. *Cell* **79**, 273–282 (1994).
34. Castel, D. et al. Dynamic binding of RBPJ is determined by Notch signaling status. *Genes Dev.* **27**, 1059–1071 (2013).
35. Jarriault, S. et al. Signalling downstream of activated mammalian Notch. *Nature* https://doi.org/10.1038/377355a0 (1995).
36. Oswald, F. et al. SHARP is a novel component of the Notch/RBP-Jκ signalling pathway. *EMBO J.* **21**, 5417–5426 (2002).
37. Oswald, F. et al. A phospho-dependent mechanism involving NCoR and KMT2D controls a permissive chromatin state at Notch target genes. *Nucleic Acids Res.* **44**, 4703–4720 (2016).
38. Delacher, M. et al. Rbpj expression in regulatory T cells is critical for restraining T2 responses. *Nat. Commun.* **10**, 1621 (2019).
39. Zheng, Y. et al. Role of conserved non-coding DNA elements in the Foxp3 gene in regulatory T-cell fate. *Nature* **463**, 808–812 (2010).
40. Feng, Y. et al. Control of the inheritance of regulatory T cell identity by a *cis* element in the Foxp3 locus. *Cell* **158**, 749–763 (2014).
41. Li, X., Liang, Y., LeBlanc, M., Benner, C. & Zheng, Y. Function of a Foxp3 *cis*-element in protecting regulatory T cell identity. *Cell* **158**, 734–748 (2014).
42. Kawakami, R. et al. Distinct Foxp3 enhancer elements coordinate development, maintenance, and function of regulatory T cells. *Immunity* **54**, 947–961.e8 (2021).
43. Dikiy, S. et al. A distal Foxp3 enhancer enables interleukin-2 dependent thymic T$_{reg}$ cell lineage commitment for robust immune tolerance. *Immunity* **54**, 931–946.e11 (2021).
44. Ohkura, N. et al. T cell receptor stimulation-induced epigenetic changes and Foxp3 expression are independent and complementary events required for T$_{reg}$ cell development. *Immunity* **37**, 785–799 (2012).
45. Mikami, N. et al. Epigenetic conversion of conventional T cells into regulatory T cells by CD28 signal deprivation. *Proc. Natl Acad. Sci. USA* **117**, 12258–12268 (2020).
46. Yue, X. et al. Control of Foxp3 stability through modulation of TET activity. *J. Exp. Med.* **213**, 377–397 (2016).
47. Schmidt, A., Eriksson, M., Shang, M.-M., Weyd, H. & Tegnér, J. Comparative analysis of protocols to induce human CD4$^+$Foxp3$^+$ regulatory T cells by combinations of IL-2, TGF-β, retinoic acid, rapamycin and butyrate. *PLoS ONE* **11**, e0148474 (2016).
48. Sher, F. et al. Rational targeting of a NuRD subcomplex guided by comprehensive in situ mutagenesis. *Nat. Genet.* **51**, 1149–1159 (2019).
49. Yuan, Z. et al. Structural and functional studies of the RBPJ-SHARP complex reveal a conserved corepressor binding site. *Cell Rep.* **26**, 845–854.e6 (2019).
50. Heinzel, T. et al. A complex containing N-CoR, mSin3 and histone deacetylase mediates transcriptional repression. *Nature* **387**, 43–48 (1997).
51. Mimitou, E. P. et al. Scalable, multimodal profiling of chromatin accessibility, gene expression and protein levels in single cells. *Nat. Biotechnol.* **39**, 1246–1258 (2021).
52. Skene, P. J. & Henikoff, S. An efficient targeted nuclease strategy for high-resolution mapping of DNA binding sites. *eLife* **6**, e21856 (2017).
53. Liu, N. et al. Direct promoter repression by BCL11A controls the fetal to adult hemoglobin switch. *Cell* **173**, 430–442.e17 (2018).
54. van der Veeken, J. et al. The transcription factor Foxp3 shapes regulatory T cell identity by tuning the activity of *trans*-acting intermediaries. *Immunity* **53**, 971–984.e5 (2020).
55. Zhou, P. et al. Single-cell CRISPR screens in vivo map T cell fate regulomes in cancer. *Nature* **624**, 154–163 (2023).
56. Meyer Zu Horste, G. et al. RBPJ controls development of pathogenic Th17 cells by regulating IL-23 receptor expression. *Cell Rep.* **16**, 392–404 (2016).
57. Chen, X. et al. Joint single-cell DNA accessibility and protein epitope profiling reveals environmental regulation of epigenomic heterogeneity. *Nat. Commun.* **9**, 4590 (2018).
58. Baskar, R. et al. Integrating transcription-factor abundance with chromatin accessibility in human erythroid lineage commitment. *Cell Rep. Methods* **2**, 100188 (2022).

Methods

Cell culture

Frozen healthy donor peripheral blood mononuclear cells (PBMCs) and cord blood CD45RA$^+$CD4$^+$ T cells were obtained from Cellular Technology or StemCell Technologies and processed immediately after thawing. For separation of naive/effector CD4$^+$ T_{conv} cells or T_{reg} cells from PBMCs, CD4$^+$ T cells were first enriched by the CD4$^+$ T Cell Isolation Kit (Miltenyi Biotec). For each cell population, CD4$^+$CD25$^-$CD45RA$^+$ naive T_{conv} cells, CD4$^+$CD45RA$^-$ effector/memory T_{conv} cells and CD4$^+$CD127^{low}CD25^{high} T_{reg} cells were sorted on a BD FACSAria III or a BD FACSAria Fusion system. T cell culture medium was composed of RPMI-1640 (Nacalai Tesque), 10% of Hyclone heat-inactivated FBS (Cytiva), 2 mM GlutaMAX, 1 mM sodium pyruvate, 0.1 mM non-essential amino acids, 55 μM β-mercaptoethanol, 100 U ml^{-1} penicillin, 100 μg ml^{-1} streptomycin and 10 mM HEPES (Gibco).

Mice for validation

Mice were housed at the Animal Resource Center for Infectious Diseases of Osaka University with a 12-h light–dark cycle, and mice were kept at a temperature of 21.5–24.5 °C with humidity ranging from 30% to 60%. B6 *Foxp3*^{hCD2}*CD4*^{Cre} mice[59,60] were crossed with *H11*$^{LSL\text{-}Cas9}$ mice[61] to generate *Foxp3*^{hCD2}*H11*$^{LSL\text{-}Cas9}$*CD4*^{Cre} mice used for the mouse validation experiments. *H11*$^{LSL\text{-}Cas9}$ (#026816) and CD4–Cre (#022071) mice were purchased from The Jackson Laboratory. The *Rbpj*$^{flox/flox}$ mouse strain (RBRC01071)[62] was provided by RIKEN BRC through the National BioResource Project of the MEXT/AMED, Japan and crossed with *Foxp3*^{hCD2} to generate B6 *Rbpj*$^{flox/flox}$*Foxp3*^{hCD2} mice. All procedures were performed in accordance with the National Institutes of Health Guide for the Care and Use of Laboratory Animals[63] and approved by the Committee on Animal Research of Osaka University.

FOXP3 induction in CD4$^+$ T cells

For FOXP3 induction in human cells, naive or edited CD4$^+$ T_{conv} cells were stimulated for 72 h using Dynabeads Human T-Activator CD3/CD28 (11131D, Thermo Fisher) at a 1:1 ratio and supplemented with 500 IU ml^{-1} human IL-2 (R&D Systems), 5 ng ml^{-1} human TGFβ (R&D Systems), 10 μg ml^{-1} ascorbate (Sigma-Aldrich), 10 nM ATRA (Sigma-Aldrich), 5 μg ml^{-1} anti-human IFNγ, anti-human IL-4, anti-human IL-6 and anti-human TNF (BioLegend) antibodies and 5 μg ml^{-1} anti-FasL (BioLegend) antibodies in complete culture medium. In some experiments, 2 μM of GapmeR ASOs (Qiagen) or 0.0001-10 μM chemical inhibitors, LY411575, DAPT, LY450139, RO4929097 and YO-01027 (Selleck) were added.

For mouse cells, edited CD4$^+$ T_{conv} cells were seeded at a density of 5×10^5 cells per millilitre and stimulated for 72 h using plate-bound 10 μg anti-CD3e (clone 145-2C11, BD) in polarizing medium containing 100 IU ml^{-1} IL-2, 1 μg ml^{-1} ascorbate, 5 μg ml^{-1} anti-IL4 monoclonal antibody, 5 μg ml^{-1} anti-IFNγ, 1 μg ml^{-1} anti-IL-6 monoclonal antibody, 10 μg ml^{-1} anti-FasL monoclonal antibody and indicated amounts of TGFβ. In some experiments, polarized cells were additionally supplemented with plate-bound 5 μg anti-CD28 (clone 37.51, BD).

Flow cytometry

For flow cytometric analysis, cells were stained with appropriate antibodies for cell-surface proteins and Live/Dead dye. Cells were fixed and permeabilized using the FOXP3/Transcription Factor Staining Buffer Set (Thermo Fisher), followed by intracellular staining. Stained cells were analysed or sorted on the BD FACSCelesta, BD FACSAria fusion or FACSAria III systems and collected using FACSDiva software (v9.1, BD Biosciences). A list of antibodies used can be found in Supplementary Table 6 under the 'FACS antibodies' tab.

Viral production and transduction

Lentivirus was produced by co-transfecting Lenti-X 293T (632180, Takara; validated by Takara) with sgRNA library plasmids, psPAX2 (Addgene plasmid #12260) and pCMV-VSV-G (Addgene plasmid #8454) using Lipofectamine 3000 (L3000015, Thermo Fisher) per the manufacturer's recommendations. Lentiviral particles were collected 48 h and 72 h post-transfection and stored at −80 °C until use. For overexpression experiments, AM-tagged (C terminus) wild-type and mutant RBPJ were ordered as gene fragments (IDT) and cloned into pXR001 (Addgene plasmid #109049) using the restriction enzymes BsiWI and NheI. The eGFP mock control plasmid was synthesized by replacing puromycin in pLVSIN-EF1a-puro (6186, Takara) with an IRES–eGFP cassette by In-Fusion cloning (639650, Takara). These plasmids were co-transfected with psPAX2 and pCMV-VSV-G for lentivirus production.

Retrovirus pseudotyped with the ecotropic envelope was used for infection of gRNA into mouse T cells. In brief, retroviral particles were generated by transfection of a SIN-retroviral vector with an U6 promoter-driven sgRNA cassette and dsRED2 fluorescent protein marker into the PLAT-E[64] cell line (a gift from T. Kitamura and commercially available from Cell BioLabs) with Lipofectamine 3000 (L3000015, Thermo Fisher). Viral particles were collected on 48 h and 72 h post-transfection. For Cre overexpression experiments, Thy1.1 control or Thy1.1-T2A–Cre gene fragments were synthesized (Twist Biosciences) and subcloned into the pMCs-IG retroviral vector (a gift from T. Kitamura), replacing the original IRES–eGFP cassette. Ecotropic-pseudotyped retroviral particles were produced as described above.

For infection of both human and mouse activated T cells and iT_{reg} cells, titred amounts of lentivirus or retrovirus were used 24 h post-activation. Cells were spinfected by centrifugation at 1,220*g* for 90 min at 32 °C. Both Lenti-X 293T and PLAT-E cell lines were validated as mycoplasma-free by suppliers and expanded at low passage frequency before cryopreservation.

Genome-wide CRISPR knockout screening

Naive CD4$^+$ T_{conv} cells were acquired from cord blood CD45RA$^+$CD4$^+$ T cells after depleting CD25$^+$ cells using CD25 MicroBeads II (Miltenyi Biotec; day 0). Cells were stimulated with plate-bound anti-human CD3 (10 μg ml^{-1}; clone UCHT1) and transduced with titrated lentivirus (at multiplicity of infection of 0.3) encoding the sgRNA library 24 h post-stimulation (day 1). This sgRNA library targeted 19,114 genes, with 77,441 sgRNA species (custom oligo library ordered from Genscript) overlapping those in the Brunello library[15], but also included an additional 50 control sgRNAs targeting the *FOXP3*-coding region and was cloned into lentiGuide-Puro (Addgene plasmid #52963) with puromycin replaced with dsRED2 (Takara) for compatibility with sorting by flow cytometry. Forty-eight hours after infection, transduced cells were collected and resuspended with freshly prepared medium including 500 IU ml^{-1} of human IL-2 (day 3) and expanded for 6 days. On day 9, resting cells were resuspended in P2 primary nucleofection buffer (Lonza) at 2×10^7 cells per 100 μl per cuvette and electroporated with 50 μg per cuvette of Cas9 protein (632641, Takara) using the pulse code EH-100 on a Lonza Nucleofector 4D. The cells were further expanded for a week and edited T cells were sorted based on RFP expression (day 18). More than 100 million RFP$^+$ cells were collected and stimulated with T_{reg}-inducing conditions to maintain a library coverage of at least 1,000 cells per sgRNA. Seventy-two hours after stimulation, cells were stained with the Zombie-Aqua Fixable dye (BioLegend) Live/Dead indicator and anti-FOXP3–APC (clone 236A/E7, Invitrogen). Cells were categorically binned by the top 15% and bottom 15% of FOXP3 expression (FOXP3^{high} and FOXP3^{low}, respectively) and sorted on a BD FACSAria III system.

Sorted cells were reverse crosslinked by incubation at 65 °C in reverse-crosslinking buffer (50 mM Tris HCl (pH 7.5), 200 mM NaCl, 10 mM EDTA and 1% SDS) with agitation overnight. On the next day, genomic DNA was extracted using the Quick-DNA Midiprep Plus Kit (D4075, Zymo Research) as per the manufacturer's recommendations. Subsequent library amplification was performed as previously described[65]. Gel-extracted next-generation sequencing-compatible

PCR products were purified using Agencourt AMPure XP SPRI beads (A63880, Beckman Coulter) before sequencing on the Illumina NextSeq500 platform.

Raw fastq files were processed through the MAGeCK (v0.5.9.5)[16] pipeline to quantify and test for guide enrichment. The raw output of MAGeCK guide-level and gene-level enrichments can be found in Supplementary Table 1. For Gene Ontology enrichment analyses, we took positive and negative regulators from the MAGeCK output with a FDR threshold of less than 0.15 and used the resulting genes as input for Metascape[66]. For GSEA analysis (Extended Data Fig. 1d), we used the LFC values obtained from the output of the MAGeCK pipeline as input for enrichment with the fgsea[67] package. Annotated positive and negative FOXP3 regulators were taken from a previous study[13] and used as the reference gene annotation database.

Cas9 RNP preparation and electroporation

RNP complexes were prepared as previously described[51]. In brief, 400 µM CRISPR RNAs (crRNAs) and trans-activating crRNAs (tracrRNAs; Integrated DNA Technologies) were mixed at a 1:1 vol/vol ratio and heated at 95 °C for 5 min. Following an incubation period of 15 min at room temperature, 30 µg Cas9 protein (632641, Takara) was added to 2.7 µl of 200 µM gRNA complex, and then incubated for over 15 min at room temperature before use. Pooled RNPs with two different gRNAs were also used in this study to maximize knockout efficiency of the target protein[20]. In this case, half the amount of gRNA complex and Cas9 protein was used for preparing each RNP complex and then mixed at a 1:1 ratio. For electroporation, pre-activated $CD4^+$ T cells were resuspended in P2 primary nucleofection buffer at 2×10^6 cells per 20 µl and mixed with RNPs in a 16-well cuvette plate. The cell-containing mixture was pulsed with the EH-100 program, and electroporated cells were cultured at $1–2 \times 10^6$ cells per millilitre in complete medium supplemented with 500 IU ml IL-2 for 4–6 days, before use in downstream assays. A list of all crRNAs used in this study can be found in Supplementary Table 5.

Cell preparation for the Perturb-icCITE-seq screen

Cell preparation for the screen was conducted essentially as the whole-genome screen described above, with the following changes. The sgRNA library encompassing 907 different gRNAs (Twist Bioscience) was cloned into a modified CROP-seq-opti vector (Addgene plasmid #106280) with the puromycin selection marker replaced with tagBFP fluorescent protein to enable flow cytometry-based cell enrichment. After expansion and polarization with T_{reg}-inducing conditions, live cells were sorted on the basis of BFP expression and stained with TotalSeq-A hashtag antibodies (BioLegend; Supplementary Table 6) as per the manufacturer's recommendations. Hashed cells were then pooled and blocked with TruStain FcX (4223020, BioLegend) before staining with a TotalSeq-A barcoded surface antibody panel (BioLegend; Supplementary Table 6) for 30 min on ice. Stained cells were washed three times before proceeding with fixation with the icCITE-seq protocol.

Perturb-icCITE-seq library preparation

Perturb-icCITE-seq libraries were prepared essentially as previously described[24]. In brief, approximately 1 million stained cells were resuspended with Cell Staining Buffer (420201, BioLegend), transferred into a 15-ml Falcon tube and then pelleted by centrifugation for 5 min at 500*g*. The supernatant was removed, leaving around 50 µl residual volume. Cell pellet was thoroughly resuspended in the residual liquid. Cells were fixed and permeabilized by dropwise addition of 1 ml pre-chilled True-Phos Perm Buffer (425401, BioLegend) while vortexing, and then incubated overnight at −20 °C.

On the next day, fixed cells were equilibrated on ice and then centrifuged at 4 °C at 2,000*g* for 5 min. Pelleted cells were gently washed with 2 ml ice-cold Intracellular Wash Buffer (1×) with 2 mM dithiothreitol and 0.2 U μl^{-1} Protector RNase Inhibitor (3335402001, Roche). The centrifugation step was repeated again to completely remove the supernatant. Intracellular staining was then performed using Intracellular Wash Buffer (1×; custom part no. 900002577, BioLegend), with the addition of 2 mM dithiothreitol, TruStain FcX (4223020, BioLegend), True Stain Monocyte Blocker (426102, BioLegend) and 1 U μl^{-1} Protector RNase Inhibitor (3335402001, Roche) in a 100 µl volume, as per the manufacturer's recommendations. Stained cells were washed three times with 1 ml of Intracellular Wash Buffer (1×), and then resuspended and counted in Intracellular Wash Buffer (1x) with 2 mM dithiothreitol and 0.2 U μl^{-1} RNase inhibitor. A maximum of 4 µl of the cell suspension was used for processing with the Chromium Next GEM Single Cell 3′ Kit v3.1 (1000268, 10X Genomics) and 3′ Feature Barcode Kit (1000262, 10X Genomics) according to the manufacturer's protocols. Use of over 4 µl will inhibit the reverse transcription reaction.

CROP-seq gRNA libraries were enriched by a two-step DialOut PCR protocol, essentially as previously described[27]. Up to three enrichment PCRs per Gel Beads-in-emulsion (GEMs) reaction were performed to maximize CROP-seq library complexity. TotalSeq-A hashtag and surface antibody libraries were prepared as per the manufacturer's recommendations (BioLegend). TotalSeq-B intracellular antibody libraries were prepared as per the guidelines outlined in the Chromium Single Cell 3′ Reagent Kits User Guide (v3.1 Chemistry) with Feature Barcoding Technology for Cell Surface Protein (CG000206, 10X Genomics, User Guide). Resulting libraries were sequenced on the Illumina NovaSeq6000 platform.

RNA-seq

RNA was extracted using the miRNeasy micro kit (Qiagen) from resting T_{conv} cells, resting nT_{reg} cells and edited iT_{reg} cells. The quality of the RNA was assessed using an RNA 6000 Pico Kit on the 2100 Bioanalyzer System (Agilent Technologies). All sequenced samples had an RNA integrity number (RIN) of more than 8. RNA-seq libraries were prepared using the Smart-seq HT kit (634455, Takara) in combination with the Nextera XT DNA Library Preparation Kit (FC-131-1096, Illumina) following the manufacturer's instructions. Sequencing was performed on the NovaSeq6000 platform (Illumina).

icRNA-seq

Cell fixation, permeabilization and rehydration were essentially as described for Perturb-icCITE-seq in the previous section. Blocking was performed with Intracellular Wash Buffer (1×; custom part no. 900002577, BioLegend), with the addition of 2 mM dithiothreitol, 2.5 µl TruStain FcX (4223020, BioLegend), 2.5 µl True Stain Monocyte Blocker (426102, BioLegend) and 1 U μl^{-1} Protector RNase Inhibitor (3335402001, Roche) in a 50 µl volume per 1 million cells and incubated on ice for 10 min. Intracellular staining was performed using anti-FOXP3 (320214, BioLegend) with a 1:50 dilution for 45 min on ice. Stained cells were washed twice with 1 ml of Intracellular Wash Buffer (1×), and then resuspended and filtered for flow cytometry in Intracellular Wash Buffer (1x) with 2 mM dithiothreitol and 0.2 U μl^{-1} RNase inhibitor. Cells were sorted directly into QIAzol (79306, Qiagen) based on intracellular FOXP3 expression. RNA extraction and library preparation were essentially as described for RNA-seq in the above section. All sequenced samples had an RIN > 8. Sequencing was performed on the NovaSeq6000 platform (Illumina).

Quantitative PCR

Quantitative PCR was performed following the manufacturer's protocol using TaqMan Fast Advanced Master Mix for quantitative PCR (Applied Biosystems) and pre-designed probes for RBPJ (Hs01068138_m1, Applied Biosystems) and ACTB (Hs01060665_g1, Applied Biosystems).

Analysis of editing efficiency

Editing efficiency of each gRNA was quantified by the tracking of indels by decomposition (TIDE) assay[68] and analysed using the inference of CRISPR edits (ICE) algorithm[69]. In brief, 5–7 days after electroporation,

2×10^5 of gene-edited cells were collected for DNA extraction using 50 µl of QuickExtract DNA Extraction Solution (QEP70750, Epicentre). PCR primers were designed to target the regions 400–600 bp flanking the predicted editing site and were subsequently amplified from extracted genomic DNA using PrimeSTAR GXL DNA Polymerase (R050A, Takara Bio). Sanger sequencing was performed by BigDye Terminator v3.1 Cycle Sequencing Kit (4337457, Applied Biosystems) and 3500xL Genetic Analyzer (Applied Biosystems). Acquired sequences were applied to ICE analysis using the web application provided by Synthego (https://ice.synthego.com/). Primers used for ICE analysis can be found in Supplementary Table 5.

CpG methylation analysis

CpG methylation of the human *FOXP3* CNS2 locus was assessed as previously described[45]. In brief, cells were collected by sorting after FOXP3 induction and staining. Following reverse crosslinking for over 20 h, DNA was extracted by NucleoSpin Tissue XS (U0901A, Takara). Bisulfite conversion was done using the EZ DNA Methylation-Lightning Kit (D5030, Zymo Research) by following the manufacturer's recommendations. Primers 5′-TTGGGTTAAGTTTGTTGTAGGATAG-3′ (forward) and 5′- ATCTAAACCCTATTATCACAACCCC-3′ (reverse) were used for PCR amplification.

In vitro FOXP3 stability assay

Edited $CD4^+$ T cells were stimulated under the iT_{reg} condition as described above and rested for 4 days with 500 IU ml^{-1} of human IL-2 and 10 µg ml^{-1} ascorbate in complete medium. FOXP3-induced cells were re-stimulated with Dynabeads Human T-Activator CD3/CD28 at a 1:1 ratio, supplemented with exogenous 100 IU ml^{-1} human IL-2 and 100 ng ml^{-1} human TNF (R&D Systems). Seventy-two hours post re-stimulation, cells were additionally rested for 4 days in the presence of human IL-2 and human TNF and then analysed for FOXP3 expression by flow cytometry.

In vitro suppression assay

In vitro suppression assays were performed by using $CD14^+$ cell-depleted PBMCs and edited iT_{reg} cells. $CD14^+$ cells were depleted in whole PBMCs by CD14 MicroBeads (Miltenyi Biotec) following the manufacturer's instructions. $CD14^+$ cell-depleted PBMCs and edited iT_{reg} cells were labelled with CellTrace Violet and CellTrace Far Red cell Proliferation Kit (Thermo Fisher), respectively, as per the manufacturer's instructions. Labelled PBMCs (1×10^5) were co-cultured with edited iT_{reg} cells at a indicated ratios in PRIME-XV T Cell Expansion XSFM (Irvine Scientific) supplemented with 10 IU ml^{-1} human IL-2 and 1 µg ml^{-1} anti-CD3 antibodies for 6 days. Cell division of $CD4^+$ or $CD8^+$ cells was assessed by flow cytometry.

Dense mutagenesis screen of *RBPJ*

A focused library including all possible exon-targeting *RBPJ* gRNAs (Twist Bioscience) was cloned, essentially as described for the whole-genome screening library. This library encompassed 151 *RBPJ*-targeting gRNA species with 20 NTCs. The screen was conducted as previously described for the whole-genome screen, using 3×10^6 cells as input with an infection multiplicity of infection of 0.3. The screen was conducted separately for three biologically independent donors. Sequenced data were processed using the CRISPRO (v1.0.1)[70] pipeline to map the FOXP3 enrichment score to protein coordinates and identify associated protein structural domains. The raw CRISPRO output of sgRNA enrichment and associated amino acid coordinates can be found in Supplementary Table 4.

Co-immunoprecipitation and western blot

iT_{reg} cells (4×10^6) transduced with lentiviral particles with either wild-type RBPJ–AM or F235A/L362A-mutant RBPJ–AM were collected and stored at −80 °C until use. Nuclear extracts were prepared by using the Universal Magnetic Co-IP Kit (Active Motif) as per the manufacturer's recommendations. For immunoprecipitation, anti-AM antibody (61677, Active Motif) or mouse IgG2a isotype control (Medical & Biological laboratories) were conjugated with HM protein G beads (Tamagawa Seiki). Nuclear lysates were incubated for 4 h at 4 °C with 1 µg antibody-conjugated beads. Antibody-conjugated beads were washed four times and resuspended with 1× sample buffer, followed by incubation at 95 °C for 5 min. Immunoblotting was performed on a Simple Western JESS system (ProteinSimple) using the software Compass for SW (v6.1.0). Anti-RBPJ antibody (clone ERP13479, Abcam) and anti-HDAC3 antibody (clone D201K, Cell Signaling Technology) were used for blotting.

EMSA

Nuclear lysate of RBPJ-overexpressed iT_{reg} cells was prepared as described in the previous section. The reaction buffer (LightShift Chemiluminescent EMSA Kit, 20148, Thermo Fisher) consisted of 1× binding buffer, 0.5% glycerol, 5 mM $MgCl_2$, 50 ng $µl^{-1}$ poly(dI:dC) and 0.05% NP-40. Probe sequences were as follows: 5′-CATCATAAAGCGTGGGAACTTAACATCAT-3′ (RBPJ consensus sequence) and 5′-GATACGTGACAGTTTCCCACAAGCCAGGCT-3′ (*FOXP3* promoter). The 3′-biotinylated probes were annealed in a duplex buffer (100 mM potassium acetate and 30 mM HEPES, pH 7.5) by heating at 95 °C for 5 min followed by gradually cooling at 1 °C per minute for 70 min. Nuclear lysate was incubated with 25 pM double-stranded probe for 30 min at room temperature. To evaluate the involvement of RBPJ protein, 0.2 µg anti-RBPJ antibody (clone 1F1, Active Motif) was added to the mixture. After incubation, the mixture was electrophoresed at 100 V for 60 min in a 6% polyacrylamide gel, and then transferred to a nylon membrane at 100 V for 30 min followed by UV-light crosslinking at 120 mJ cm^{-2} for 1 min. The crosslinked DNA was then detected by using the Chemiluminescent Nucleic Acid Detection Module Kit (Thermo Fisher) and the AI600 Chemiluminescent Imager (Cytiva).

Luciferase assay

To construct the luciferase reporter plasmid, wild-type, RBPJ-binding motif-deleted (ΔRBPJ) or RBPJ-binding motif-mutated (A→G mutation) *FOXP3* promoter region (455 bp: −389 to approximately +66) were cloned into the pNL1.1 vector (Promega). Pre-activated $CD4^+$ T cells were resuspended in P3 primary nucleofection buffer (Lonza) at 2×10^6 cells per 20 µl, mixed with 2 µg of plasmid and then pulsed with the EO-115 program. Electroporated cells were immediately transferred to pre-warmed culture medium including 500 IU ml^{-1} IL-2 at a concentration of 1×10^6 cells per millilitre. Resulting cells were cultured for 24 h and then stimulated with FOXP3-inducing conditions as described above. Luciferase activity was analysed 24 h after stimulation using the Nano-Glo Luciferase Assay System (Promega) and Cytation 5 Cell Imaging Multi-Mode Reader (Agilent). Relative luminescence units were calculated by using unstimulated cells electroporated with a vector harbouring the wild-type *FOXP3* promoter as a baseline.

ChIP–seq library preparation and sequencing

Sorted cells were fixed with 1% PFA for 10 min at room temperature and then quenched with glycine. Fixed cells were then centrifuged at 600*g* for 5 min at 4 °C and the supernatant was removed. Cell pellets were stored at −80 °C until use. Cell pellet was thawed and resuspended in 100 µl nuclear lysis buffer (50 mM Tris-HCl (pH 7.5), 10 mM EDTA and 1% SDS), supplemented with 1× protease inhibitor cocktail (11873580001, Roche) and incubated on ice for 10 min. Sonication was performed on the Picorupter platform (Diagenode) for five cycles of 30 s ON–30 s OFF. Sheared chromatin was centrifuged at 10,000*g* for 10 min at 4 °C and the clarified supernatant was transferred to a DNA LoBind Eppendorf tube (Eppendorf). ChIP was performed using the iDeal ChIP-seq kit for histones (C01010173, Diagenode) as per the manufacturer's recommendations. The reverse-crosslinked reaction was column purified with

ChIP DNA Clean & Concentrator (D5205, Zymo Research), and library preparation was performed with the KAPA HyperPrep kit (KK8504, Roche) according to the manufacturer's instructions. Libraries were sequenced on the NextSeq500 or NovaSeq platform (Illumina).

ATAC-seq library preparation and sequencing

ATAC-seq libraries were prepared by using the ATAC-Seq Kit (53150, Active Motif) following the manufacturer's instructions. In brief, 1×10^5 live sorted cells were pelleted by centrifugation at 500*g* for 5 min at 4 °C. The cell pellet was resuspended thoroughly in 100 µl ice-cold ATAC Lysis Buffer. After spinning down at 500*g* for 10 min at 4 °C, the nuclear pellet was tagmented in 50 µl of Tagmentation Master Mix at 37 °C for 30 min. For library preparation, the tagmented DNA was amplified with indexed primer by PCR following column purification. Prepared libraries were sequenced on the NovaSeq platform (Illumina).

CUT&RUN library preparation and sequencing

CUT&RUN libraries were performed essentially as previously described[54] with the modifications described below. After antibody staining, cells were washed twice with buffer 1 (1× permeabilization buffer from eBioscience Foxp3/Transcription Factor Staining Buffer Set, 1× EDTA-free protease inhibitors, 0.5 mM spermidine and 2 mM EDTA), and incubated with pA/G-MNase (40366S, CST) at 1.5 µl per 50 µl buffer 1 for 1 h on ice. After washing twice with buffer 2 (0.05% (w:v) saponin, 1× EDTA-free protease inhibitors and 0.5 mM spermidine in PBS), cells were resuspended in 100 µl calcium buffer (20 mM HEPES, 150 mM NaCl, 0.5 mM spermidine, 0.05% (w/v) saponin, 1× EDTA-free protease inhibitors and 2 mM $CaCl_2$) to activate the micrococcal nuclease. After a 30-min incubation period on ice, 100 µl of 2× stop solution (20 mM EDTA and 4 mM EGTA in buffer 2) was added, and the reaction was incubated for 10 min in a 37 °C incubator to release the cleaved chromatin fragments. 2.5 µl sample normalization spike-in DNA was added per reaction and supernatants were collected by centrifugation. DNA was purified using a Zymo DNA Clean & Concentrator-5 column (D4014, Zymo Research) and the eluted material was subjected to library preparation using the KAPA HyperPrep kit (KK8504, Roche) as previously described[54]. Libraries were sequenced on the NovaSeq platform (Illumina).

Cell fixation and permeabilization for inATAC and inChIP

Transduced cells were sorted based on an eGFP reporter and polarized to iT_{reg} cells under conditions described above. Seventy-two hours post-FOXP3 induction, live cells were enriched through flow cytometry on a BD FACSAria fusion. Cells were fixed and permeabilized as previously described[51], using the Omni lysis buffer (10 mM Tris-HCl (pH 7.4), 10 mM NaCl, 3 mM $MgCl_2$, 0.1% NP-40, 0.1% Tween-20, 0.01% digitonin and 1% BSA). Permeabilization was performed for 3 min on ice, followed by adding 1 ml chilled wash buffer (10 mM Tris-HCl (pH 7.4), 10 mM NaCl, 3 mM $MgCl_2$ and 1% BSA) and mixing by inversion before centrifugation at 600*g* for 5 min at 4 °C. The supernatant was discarded, and cells were resuspended in Intracellular Staining Buffer (custom part number 900002577, BioLegend), with the addition of TruStain FcX (BioLegend) and blocked for 10 min on ice and then stained with anti-human FOXP3 (clone #259D, BioLegend) at a 1:100 dilution for 45 min on ice. Following staining, the cells were washed three times with FACS staining buffer (2% BSA and 1 mM EDTA in PBS) and sorted for FOXP3 expression.

inATAC library preparation and sequencing

Approximately 1×10^5 sorted cells were pelleted by centrifugation at 600*g* for 5 min at 4 °C. After carefully removing the supernatant, the cells were gently resuspended in a Omni-ATAC[71] transposition mix (50 µl 2× TD buffer, 5 µl TDE1 enzyme (Illumina), 33 µl PBS, 1 µl 1% digitonin, 1 µl 10% Tween-20 and 10 µl water). Transposition reactions were incubated at 37 °C for 60 min in a thermomixer with shaking at 1,000 rpm. Following transposition, reactions were diluted with FACS staining buffer and centrifuged at 800*g* for 5 min at 4 °C on a swing bucket rotor. The supernatant was discarded, and cells were washed with 100 µl 1× diluted nuclei buffer (10x Genomics) and centrifuged again at 800*g* for 5 min at 4 °C on a fixed angle rotor. The supernatant was carefully removed, and transposed cells were resuspended in 30 µl 1× diluted nuclei buffer. One microlitre of 1% SDS was added, and the mixture was incubated at 37 °C for 10 min and then used directly as input for ATAC-seq library preparation as previously described[72]. Sequencing was performed on the NextSeq500 or NovaSeq platform (Illumina).

inChIP library preparation and sequencing

For each reaction, 30 µl Dynabeads protein G and protein A magnetic beads (1:1 ratio; Invitrogen) was resuspended in 500 µl bead wash buffer (0.5% BSA in PBS) and then pre-incubated with 3 µg of the appropriate antibody at 4 °C on a rotator for at least 2 h. Subsequently, the reactions were placed on a magnet and washed three times with 500 µl bead wash buffer to remove excess antibodies and then resuspended to the original bead volume with bead wash buffer.

Fixed cells were sorted and resuspended in 100 µl nuclear lysis buffer (50 mM Tris-HCl (pH 7.5), 10 mM EDTA and 1% SDS), supplemented with 1× protease inhibitor cocktail (11873580001, Roche) and incubated on ice for 10 min. Sonication was performed on the Picorupter platform (Diagenode) for five cycles of 30 s ON–30 s OFF. Sheared chromatin was centrifuged at 10,000*g* for 10 min at 4 °C, and the clarified supernatant was transferred to a new DNA LoBind Eppendorf tube. Chromatin was diluted 10× using ChIP dilution buffer (16.7 mM Tris (pH 7.5), 167 mM NaCl, 1.2 mM EDTA, 1.1% Triton X-100 and 0.01% SDS) supplemented with 1× protease inhibitor cocktail and blocked with 5 µl Fab fragment goat anti-mouse IgG (115-007-003, Jackson ImmunoResearch) on ice for at least 1 h, with occasional mixing by inversion. Note that the blocking reagents must be selected based on the isotype of the staining antibodies used in flow cytometry. The mixture was incubated overnight at 4 °C on a rotator with antibody-conjugated beads. On the next day, beads were washed and reverse crosslinked with the iDeal ChIP-seq kit for histones (C01010173, Diagenode) as per the manufacturer's recommendations and then column purified with ChIP DNA Clean & Concentrator (D5205, Zymo Research). Library preparation was performed with the KAPA HyperPrep kit (KK8504, Roche) according to the manufacturer's instructions and then sequenced on the Illumina NextSeq500 or NovaSeq6000 platform.

GvHD model and in vivo stability of iT_{reg} cells

NSG mice aged 6–8 weeks were irradiated with 2.25 Gy. Twenty-four hours post-irradiation, mice were given 2.5×10^6 human PBMCs to induce xenograft GvHD. To evaluate the effect of gene-edited iT_{reg} cells, NTC or *RBPJ*-KO iT_{reg} cells were co-transferred with human PBMCs at a 1:1 ratio. Body weight was monitored for 25–30 days after cell transplantation, and mice with weight loss greater than 20% were euthanized. To assess the in vivo stability of iT_{reg} cells, 5×10^6 gene-edited iT_{reg} cells were transferred into irradiated NSG mice. Transferred cells from peripheral blood and the spleen were analysed 5 days later.

Statistical analysis

Statistical analyses for all experiments except sequencing analyses were conducted using GraphPad Prism (v10.4.1). No statistical method was used for predetermined sample size. In vitro experiments were not performed in a blinded fashion, but were measured with objective methodologies. For in vivo experiments, measurements of weight loss and monitoring of mouse health were performed by an experimenter blinded to the experimental groups. The statistical tests used to assess significance along with biological and experimental replicates in each dataset are specified in the figure legends for each corresponding figure. No samples were excluded from the analysis. Statistical significance was defined as $P \leq 0.05$.

Reporting summary

Further information on research design is available in the Nature Portfolio Reporting Summary linked to this article.

Data availability

All CRISPR screen data reported in this paper are provided in Supplementary Tables 1 and 4. All next-generation sequencing data generated as part of this study have been deposited in the DNA Data Bank of Japan (DDBJ) Sequence Read Archive under series accession number PRJDB16517. All data have been aligned to the human reference genome GRCh38 (hg38). Source data are provided with this paper.

Code availability

The Perturb-icCITE-seq processing scripts used for this paper are available in GitHub (https://github.com/agiguelay/Perturb-icCITEseq).

59. Komatsu, N. et al. Heterogeneity of natural Foxp3$^+$ T cells: a committed regulatory T-cell lineage and an uncommitted minor population retaining plasticity. *Proc. Natl Acad. Sci. USA* **106**, 1903–1908 (2009).
60. Lee, P. P. et al. A critical role for Dnmt1 and DNA methylation in T cell development, function, and survival. *Immunity* **15**, 763–774 (2001).
61. Chiou, S. H. et al. Pancreatic cancer modeling using retrograde viral vector delivery and in vivo CRISPR/Cas9-mediated somatic genome editing. *Genes Dev.* **29**, 1576–1585 (2015).
62. Han, H. et al. Inducible gene knockout of transcription factor recombination signal binding protein-J reveals its essential role in T versus B lineage decision. *Int. Immunol.* **14**, 637–645 (2002).
63. National Research Council, Division on Earth and Life Studies, Institute for Laboratory Animal Research & Committee for the Update of the Guide for the Care and Use of Laboratory Animals. *Guide for the Care and Use of Laboratory Animals* 8th edn (National Academies Press, 2011).
64. Morita, S., Kojima, T. & Kitamura, T. Plat-E: an efficient and stable system for transient packaging of retroviruses. *Gene Ther.* **7**, 1063–1066 (2000).
65. Joung, J. et al. Genome-scale CRISPR–Cas9 knockout and transcriptional activation screening. *Nat. Protoc.* **12**, 828–863 (2017).
66. Zhou, Y. et al. Metascape provides a biologist-oriented resource for the analysis of systems-level datasets. *Nat. Commun.* **10**, 1523 (2019).
67. Korotkevich, G. et al. Fast gene set enrichment analysis. Preprint at *bioRxiv* https://doi.org/10.1101/060012 (2021).
68. Brinkman, E. K. & van Steensel, B. Rapid quantitative evaluation of CRISPR genome editing by TIDE and TIDER. *Methods Mol. Biol.* **1961**, 29–44 (2019).
69. Conant, D. et al. Inference of CRISPR edits from Sanger trace data. *CRISPR J.* **5**, 123–130 (2022).
70. Schoonenberg, V. A. C. et al. CRISPRO: identification of functional protein coding sequences based on genome editing dense mutagenesis. *Genome Biol.* **19**, 169 (2018).
71. Corces, M. R. et al. An improved ATAC-seq protocol reduces background and enables interrogation of frozen tissues. *Nat. Methods* **14**, 959–962 (2017).
72. Buenrostro, J. D., Wu, B., Chang, H. Y. & Greenleaf, W. J. ATAC-seq: a method for assaying chromatin accessibility genome-wide. *Curr. Protoc. Mol. Biol.* **109**, 21.29.1–21.29.9 (2015).
73. Akella, N. M., Ciraku, L. & Reginato, M. J. Fueling the fire: emerging role of the hexosamine biosynthetic pathway in cancer. *BMC Biol.* **17**, 52 (2019).
74. Xu, C. & Ng, D. T. Glycosylation-directed quality control of protein folding. *Nat. Rev. Mol. Cell Biol.* **16**, 742–752 (2015).

Acknowledgements We thank the members of the Sakaguchi laboratory for technical advice and discussions; S. Hori for providing FOXP3-hCD2/CD52 mice; the Genome Information Research Center of the Research Institute for Microbial Diseases at Osaka University for next-generation sequencing support; and the Research Cluster of the Berlin Institute of Health for computational support on the high-performance computing (HPC). The graphics in Fig. 5a and Extended Data Figs. 1a and 4a were created in BioRender (https://biorender.com). This research was supported by Grants-in-Aid by the Japan Society for Promotion of Science (JSPS) for Specially Promoted Research no. 16H06295 and the Japan Agency for Medical Research and Development (P-CREATE, 18cm0106303; LEAP, 18gm0010005) to S.S. and the Japan Society for the Promotion of Science (JSPS) KAKENHI Grant-in-Aid for Early-Career Scientists 23K14545 to K.Y.C.

Author contributions K.Y.C., T.K. and S.S. conceived and designed experiments with input from N.M. K.Y.C., T.K., M.H. and S.N. carried out the experiments. K.Y.C., T.K. and Y.T. carried out analyses, with substantial contributions from A.G. on the single-cell dataset. K.Y.C. conceived and designed the methods with input from T.K. and K.I. R.O. provided insights and discussions for experimental planning. L.S.L., K.H. and S.S. each supervised various aspects of the work. K.Y.C., T.K. and S.S. drafted the manuscript with input from all other authors.

Competing interests S.S. has received grant support from Chugai Pharmaceutical. T.K., R.O. and K.H. are employed by Chugai Pharmaceutical, and R.O. and K.H. also hold stocks in the company. The other authors declare no competing interests.

Additional information

Supplementary information The online version contains supplementary material available at https://doi.org/10.1038/s41586-025-08795-5.

Correspondence and requests for materials should be addressed to Kelvin Y. Chen or Shimon Sakaguchi.

Peer review information *Nature* thanks Massimiliano Pagani and the other, anonymous, reviewer(s) for their contribution to the peer review of this work.

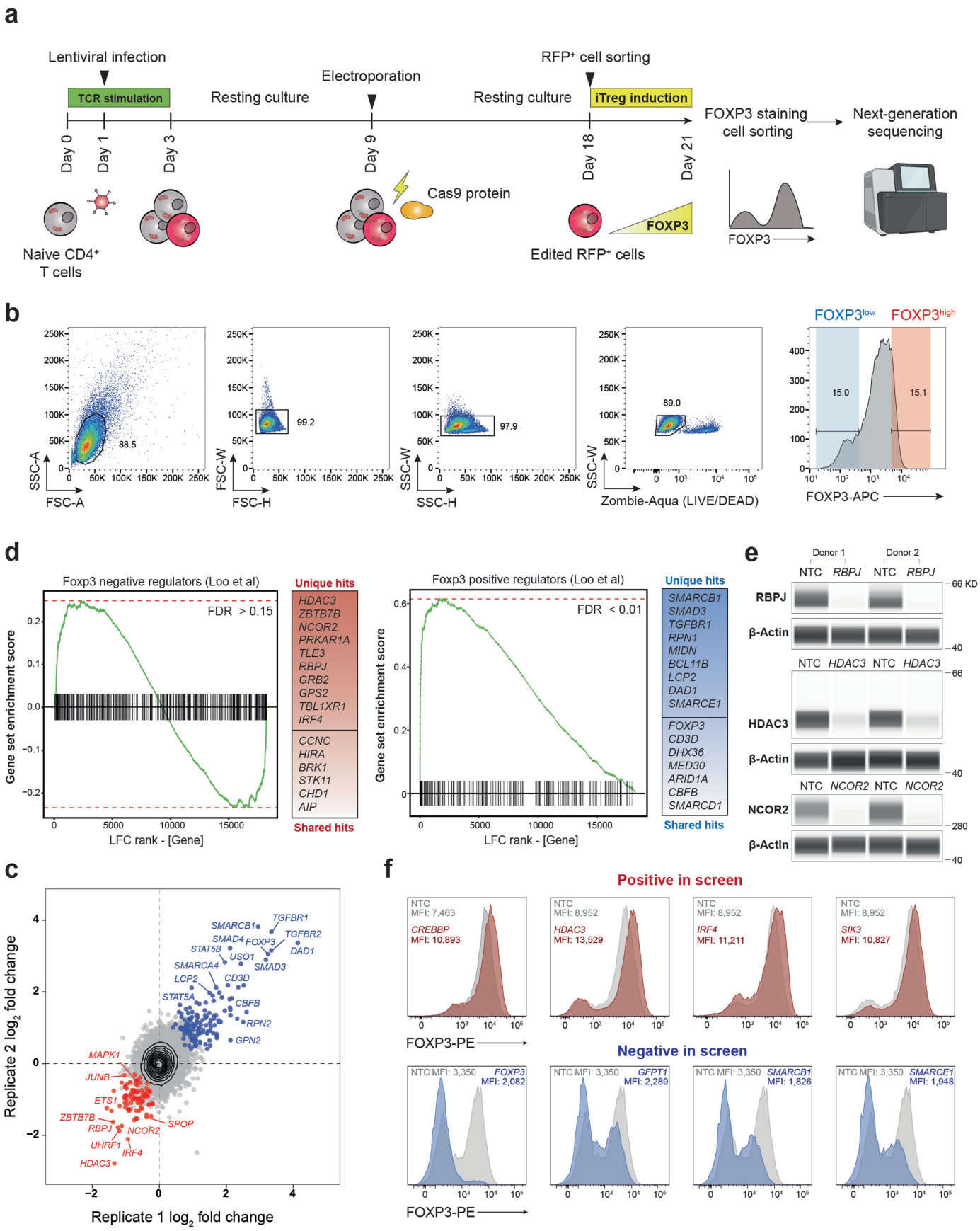

Extended Data Fig. 1 | See next page for caption.

Extended Data Fig. 1 | Design and validation of the iTreg whole-genome CRISPR screen in primary human T cells. a, Detailed timeline schematic of the CRISPR screening pipeline. The schematic of the cells was adapted from ref. 51, Springer Nature, and the graphic of the next-generation sequencing was created using BioRender (https://biorender.com). **b**, Gating strategy used for the FOXP3 screen in **a**. **c**, Scatter plot of gene-level LFC (between $FOXP3^{hi}$ and $FOXP3^{lo}$ sorting bins), comparing screens between two replicates. **d**, Gene-set enrichment analysis of top-ranked FOXP3 negative (left) and positive (right) screen hits in a curated list from a previous study[13]. FDR = False discovery rate, permutation test. Representative unique and shared hits are shown in the text-box on the right. **e**, Western Blot analysis of protein expression of RBPJ, HDAC3 and NCOR2 in cells treated with the indicated perturbations. Data is representative of two independent donors (n = 4 donors). **f**, Representative histograms depicting FOXP3 expression in iTregs with indicated genetic perturbations, related to Fig. 1e,f. Negative (red) and positive (blue) regulators are overlaid on NTC (gray). MFI, median fluorescence intensity.

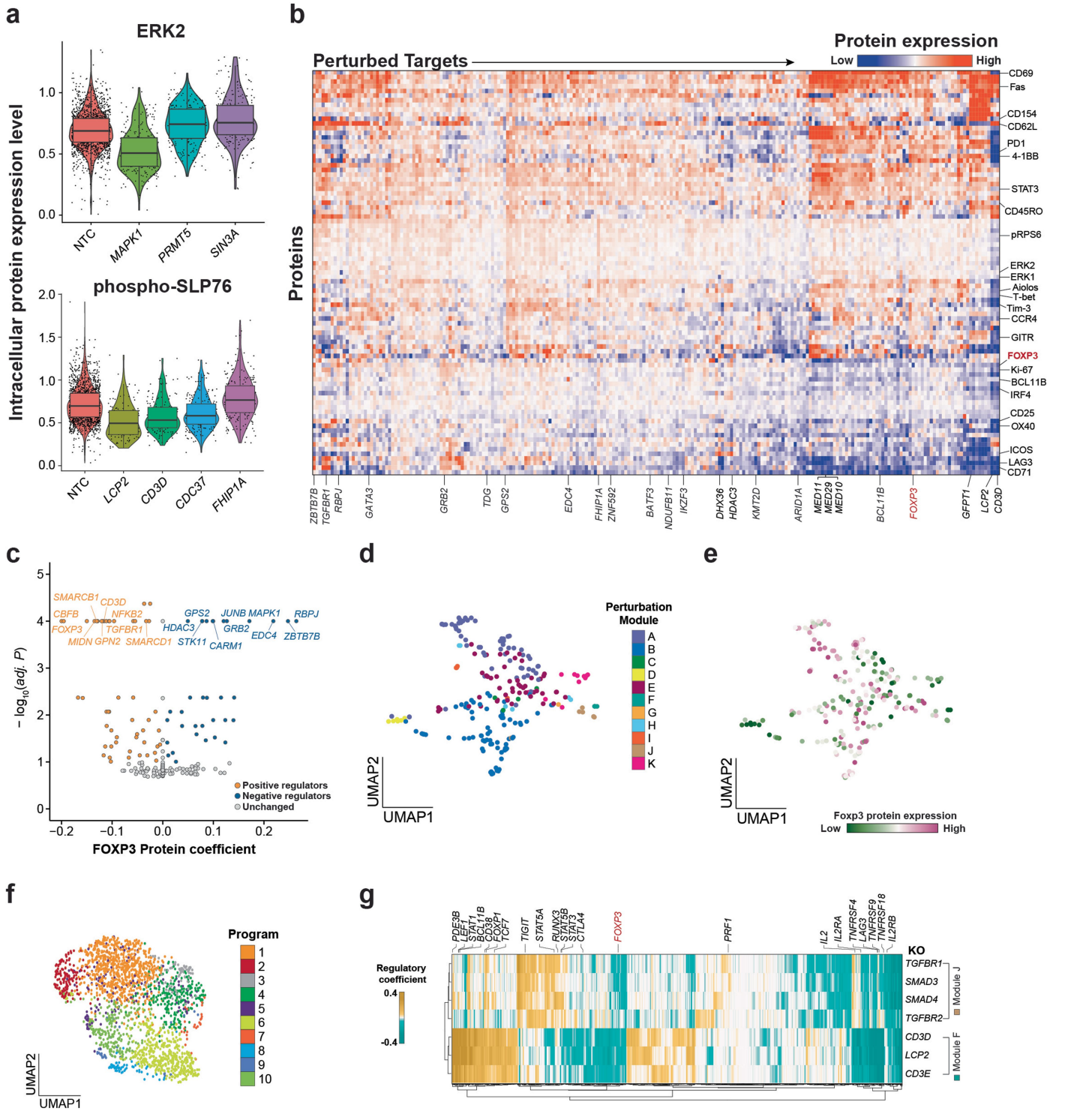

Extended Data Fig. 2 | Supporting information for gene perturbation analyses by Perturb-icCITE-seq. a, Violin plots for indicated proteins showing the distribution of protein expression for select targeted genes (KO). The boxplot spans from the first to the third quartile of the distribution, with the median positioned in the center. Whiskers represent the minimum and maximum values, excluding outliers. **b**, Heatmap showing mean expression score for select protein markers across gRNA perturbations in iTreg cells (Supplementary Table 2). **c**, Selection of significant ($p \leq 0.1$) positive (orange) and negative (blue) regulators of FOXP3 (non-null regulatory coefficient; Methods) as determined by icCITE-seq FOXP3 protein signal. The *x* axis shows FOXP3 protein coefficient and *y* axis shows $-\log_{10}$ of the adjusted *P*-value (adj. *P*) calculated using the Wilcoxon Rank-Sum test with Bonferroni correction for multiple testing. **d**,**e**, UMAP embeddings of the regulatory profiles of the 228 targeted genes, colored by their associated target module (**d**) and icCITE-seq FOXP3 protein expression score (**e**), related to Fig. 2d. **f**, UMAP embedding of the regulated profiles of 2,192 impacted genes. Color is indicative of the associated gene program (GP). **g**, Regulatory coefficient (β) values on RNA following targeted gene perturbation of indicated genes. Perturbations in the TCR and TGFβ signaling pathways. Values plotted in **a** represent cells from a single replicate.

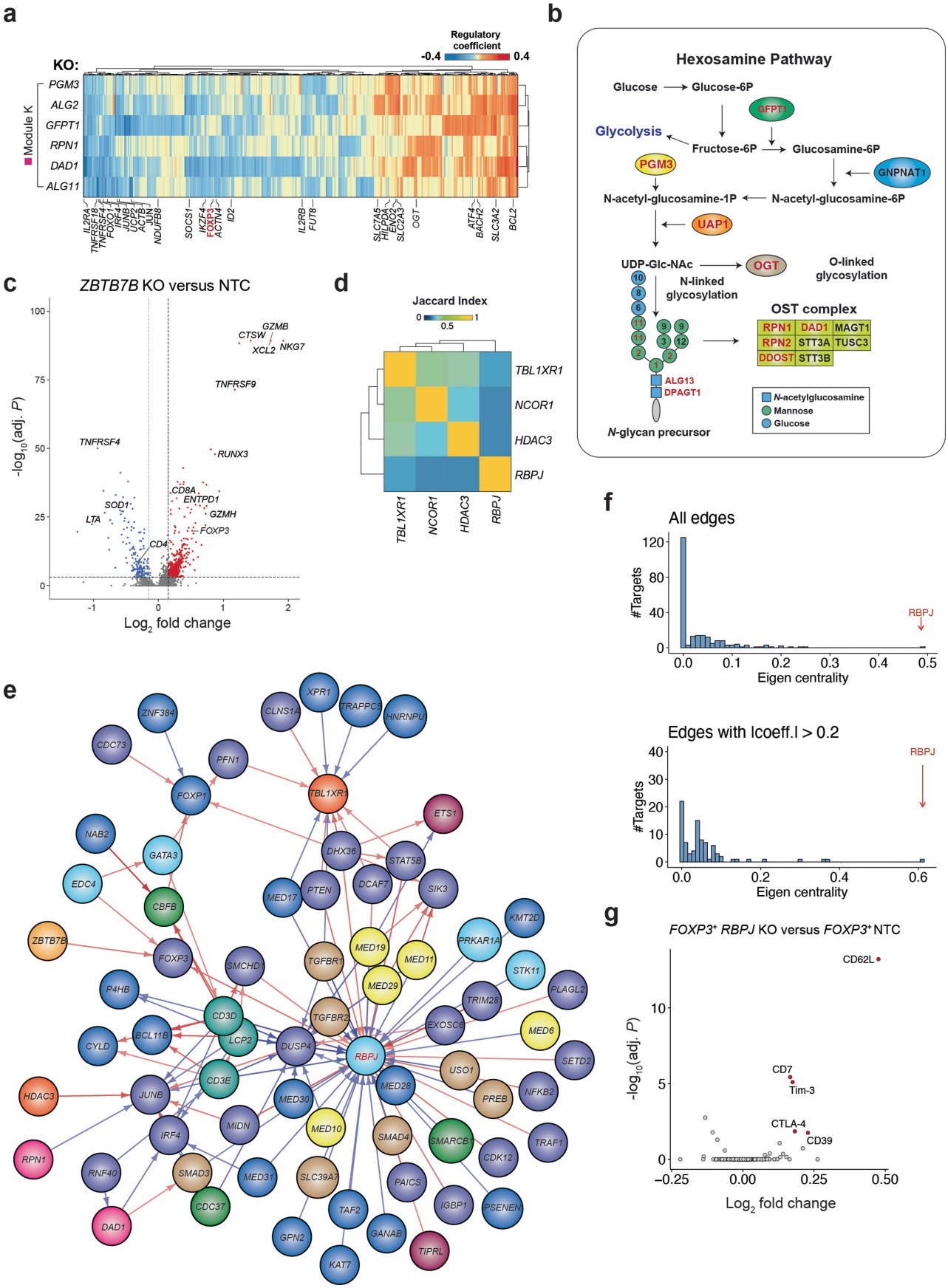

Extended Data Fig. 3 | See next page for caption.

Extended Data Fig. 3 | Elucidating perturbation-induced phenotypes with Perturb-icCITE-seq. a, Regulatory coefficient (β) values on RNA following targeted gene perturbation of indicated genes. Perturbations in the hexosamine pathways. **b**, Hexosamine signaling and downstream pathways. The graphic was adapted from refs. 73,74, Springer Nature. Gene names of ALG enzymes that mediate the assembly of mature precursor molecules are indicated by the number (e.g. *ALG1*, *ALG2*, *ALG11*, etc.). Positive regulators of FOXP3 expression as determined by the whole-genome screen are colored in red. **c**, Volcano plot of differentially regulated genes between *ZBTB7B* KO and control-edited iTreg cells as determined by Perturb-icCITE-seq. The *x* axis shows LFC and *y* axis shows $-\log_{10}$ of the adjusted *P*-value (adj. *P*) calculated using the Wilcoxon Rank-Sum test with Bonferroni correction for multiple testing. **d**, A heatmap of Jaccard similarity indexes computed on the differentially expressed genes (absolute fold-change ≥ 1.2, $p \leq 0.01$) between members of the NCOR complex. **e**, Network graph showing the major transcriptional effects (magnitude ≥ 0.2) of perturbed targets on each other. Red/blue arrows are indicative of positive/negative effects on gene expression. Arrow color is determined by the mean regulatory effect size β coefficient. **f**, Distribution of perturbed gene eigencentrality calculated on either the complete target regulatory network graph (top) or a subset (bottom, edges with an absolute coefficient ≥ 0.2, related to (**e**)). **g**, Volcano plot of differentially regulated surface proteins between FOXP3-expressing *RBPJ* KO and control-edited iTreg cells as determined by Perturb-icCITE-seq. The *x* axis shows LFC and *y* axis shows $-\log_{10}$ of the adjusted *P*-value (adj. *P*) calculated using the Wilcoxon Rank-Sum test with Bonferroni correction for multiple testing.

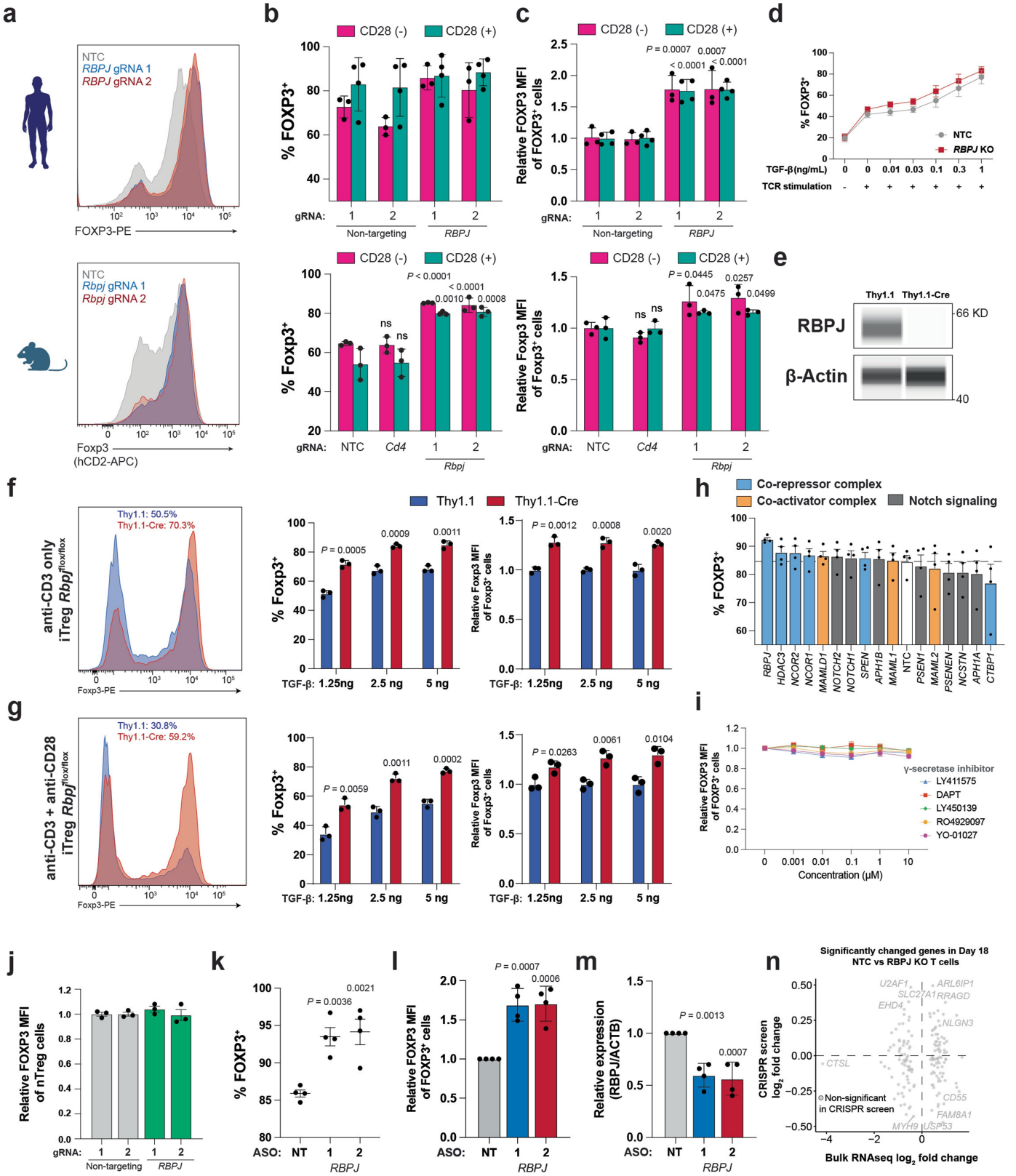

Extended Data Fig. 4 | See next page for caption.

Extended Data Fig. 4 | RBPJ is a negative regulator of FOXP3 expression in mice and humans. a, Representative histograms depicting FOXP3 expression in *RBPJ*-ablated iTregs in human (top; $n = 3$ donors) and mouse (bottom; $n = 3$ biological replicates) cells without CD28 co-stimulation. Two individual gRNAs (blue and red) are overlaid on a non-targeting control (gray). The silhouette of the human was adapted from ref. 51, Springer Nature, and the schematic of the mouse was created using BioRender (https://biorender.com). **b**, Summarized data of the experiment in (**a**), FOXP3 expression was determined by flow cytometry for human ($n = 4$ donors, CD28 + ; 3 donors CD28-) and mouse ($n = 3$ biological replicates) iTregs. **c**, Analysis of relative FOXP3 MFI in human (top) and mouse (bottom) $FOXP3^+$ iTreg cells after polarization in $CD4^+$ T cells, related to the experiment in (**a** and **b**). **d**, TGFβ dose titration analysis of FOXP3 induction in control or RBPJ-depleted human $CD4^+$ T cells ($n = 4$ donors), demonstrating its dependence in RBPJ KO cells. **e**, Western Blot analysis of protein expression of RBPJ in cells treated with the indicated perturbations. Naive $CD4^+$ T cells from $RBPJ^{flox/flox}$ mice were isolated and transduced with viral particles harboring Thy1.1-T2A-Cre or mock Thy1.1 constructs to induce knockout of the RBPJ. Data is representative of two biological replicates ($n = 2$). **f**,**g** Left, Representative histograms depicting Foxp3 expression in iTregs derived from $RBPJ^{flox/flox}$ $CD4^+$ T cells treated under the indicated conditions with (**g**) or without (**f**) CD28 co-stimulation ($n = 3$ biological replicates). Right, Summarized data of the experiment. Foxp3 expression was determined by flow cytometry. **h**, Analysis of %$FOXP3^+$ cells after iTreg polarization in human $CD4^+$ T cells with indicated genetic perturbations ($n = 4$ donors, related to the experiment in Fig. 3b). **i**, Analysis of relative FOXP3 MFI in $FOXP3^+$ iTreg cells after polarization in human $CD4^+$ T cells treated with the indicated dose of Notch signaling-related inhibitors ($n = 4$ donors). **j**, Relative FOXP3 MFI analysis in control or RBPJ-depleted human nTregs ($n = 3$ donors), showing that nTregs were only marginally affected. **k**, Summarized data ($n = 4$ donors) for the antisense oligonucleotide (ASO) experiment in (Fig. 3c; $n = 4$ donors). **l**, Statistical analysis of FOXP3 MFI in $FOXP3^+$ iTregs from the experiment in (**k**). **m**, Quantification of relative RBPJ mRNA knockdown efficiency as determined by qPCR, related to the experiment in (**k**,**l**). **n**, Scatter plot of differential gene expression fold changes from bulk RNA-seq in NTC vs. RBPJ-knockout resting T cells, along with their respective enrichment in the CRISPR screen. All data are presented as mean ± s.e.m. ns, not significant. Statistical analysis was performed with a one-way ANOVA with Dunnett's multiple comparison test for **b** (bottom), **c** and **k**-**m**, two-tailed unpaired Student's *t*-test in **f**,**g**.

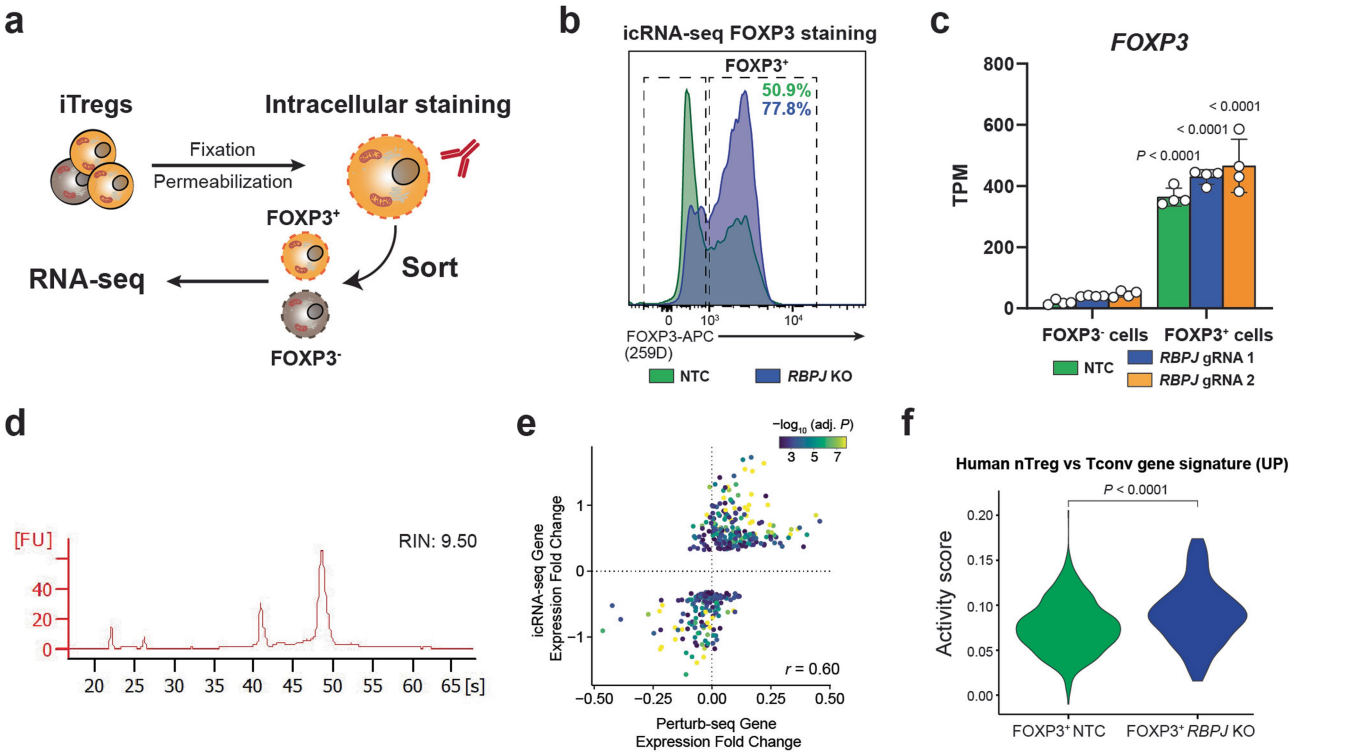

Extended Data Fig. 5 | icRNA-seq analysis of RNA expression in FACS-enriched FOXP3$^+$ cells. a, Schematic depicting the icRNA protocol (Methods). **b**, Validation of FOXP3 intracellular staining using the icRNA protocol. Data is representative of three independent trials and the antibody clone used is indicated. The schematic was adapted from ref. 51, Springer Nature. **c**, Gene expression levels for *FOXP3* measured by icRNA-seq ($n = 4$ donors, mean ± s.e.m.). Statistical analysis was performed with a two-tailed unpaired Student's *t*-test. **d**, Bioanalyzer trace depicting high-quality RNA obtained from fixed and permeabilized FACS-sorted cells. **e**, Scatter plot of gene expression fold changes from Perturb-seq and icRNA-seq in FOXP3$^+$ RBPJ-knockout vs FOXP3$^+$ NTC iTreg cells. The color is representative of the $-\log_{10}$ of the adjusted *P*-value calculated using a two-tailed Wilcoxon Rank-Sum test with Bonferroni correction for multiple testing. **f**, Activity scores of gene signatures associated with nTregs from the Perturb-icCITE-seq experiment. *P*-values by a two-tailed Wilcoxon signed-rank test.

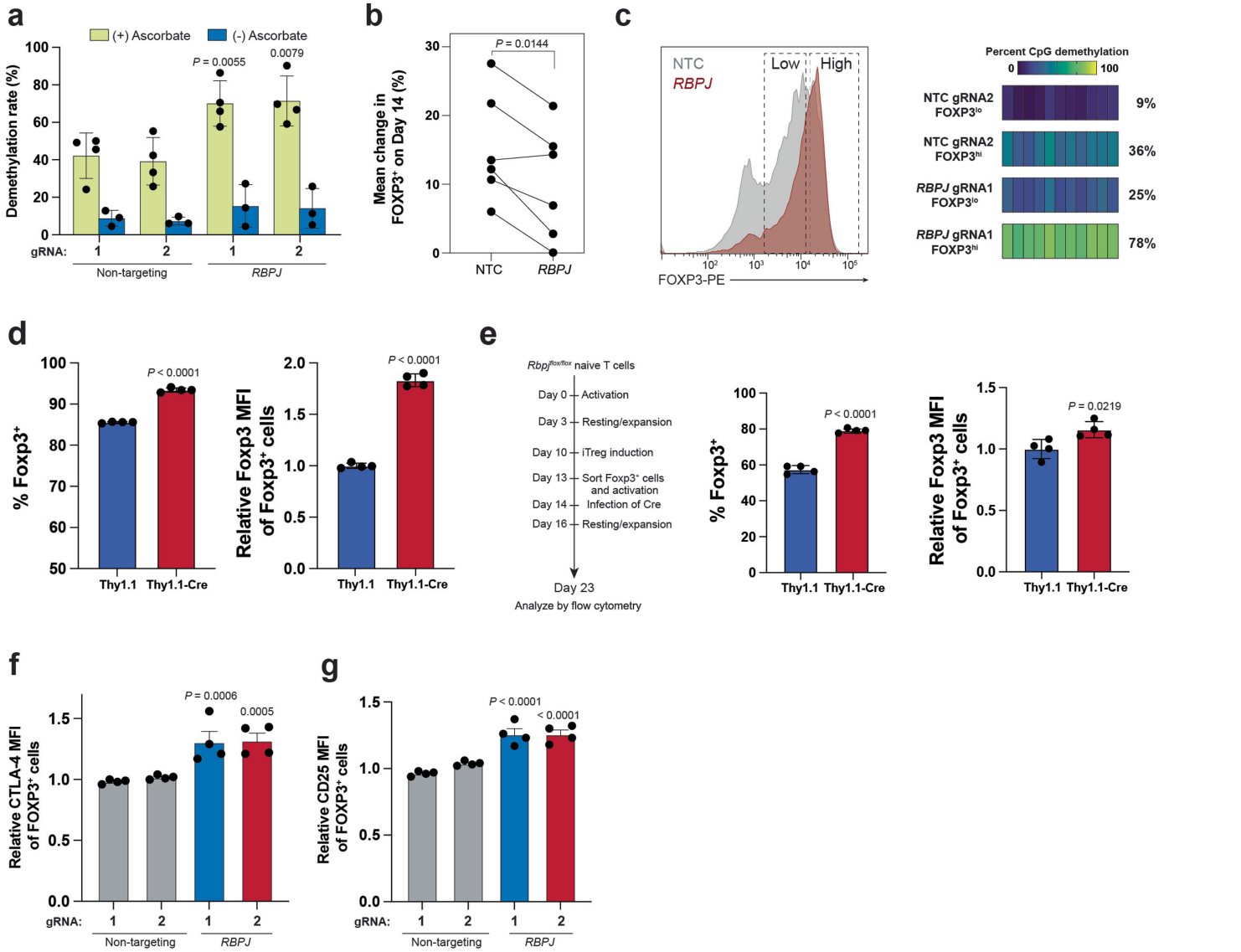

Extended Data Fig. 6 | RBPJ ablation increases iTreg stability. a, Summarized DNA demethylation rate across *FOXP3* CNS2 ($n = 4$ donors for (+)Ascorbate; 3 donors for (-) Ascorbate) from RBPJ-KO iTregs and non-targeting controls, related to the experiment in (Fig. 3g). For statistical assessment, the donor-level demethylation rate of NTC gRNA 1 and 2 were averaged compared to each *RBPJ* gRNA species. **b**, Statistical analysis of the mean change of FOXP3$^+$ cells in control or RBPJ-ablated iTregs on Day 14 ($n = 6$ donors), related to the experiment in (Fig. 3h,i). Mean change was measured by averaging the change in FOXP3$^+$ Day 14 versus Day 7 per donor in both gRNA species for control and *RBPJ*. **c**, Left, Gating strategy used for the experiment in (Fig. 3h,i). FOXP3^{hi} and FOXP3^{lo} cells were sorted and subjected to bisulfite sequencing at *FOXP3* CNS2 to assess DNA demethylation rate. The heatmap (right) shows summarized DNA methylation status at each of the 11 CNS2 CpGs across eight independent donors. **d**, Foxp3 stability assessed in iTreg cells derived from RBPJ$^{flox/flox}$/Foxp3-hCD2 reporter mice. Naive CD4$^+$ T cells from mice were isolated and transduced with viral particles harboring Thy1.1-T2A-Cre or mock Thy1.1 constructs to induce knockout of the RBPJ and cultured under iTreg polarizing conditions. Foxp3$^+$ iTregs were sorted to purity by flow cytometry and cultured for seven days in the presence of IL-2 before analysis. Analysis of %Foxp3$^+$ cells (left) and relative Foxp3 MFI (right) at the end of culture ($n = 4$ biological replicates). **e**, Assessment of the effect of *Rbpj* knockout in Foxp3 lineage-committed mouse iTregs. Left, Schematic of experiment for assessing in vitro Foxp3 stability. Foxp3$^+$ iTregs were sorted by flow cytometry and retrovirally transduced with constructs expressing Thy1.1-T2A-Cre or mock Thy1.1. Thy1.1$^+$ were rested and cultured for an additional seven days before analysis. Analysis of %Foxp3$^+$ cells (middle) and relative Foxp3 MFI (right) at the end of culture ($n = 4$ biological replicates). **f**,**g**, Relative CTLA-4 (**f**) and CD25 (**g**) MFI analysis in control or *RBPJ*-ablated human FOXP3$^+$ iTregs ($n = 4$ donors). All data are presented as mean ± s.e.m. ns, not significant. Repeated measures one-way ANOVA with Dunnett's multiple comparison test for **a** and **f**,**g**; two-tailed paired and unpaired Student's *t*-test in **b** and **d**,**e**, respectively.

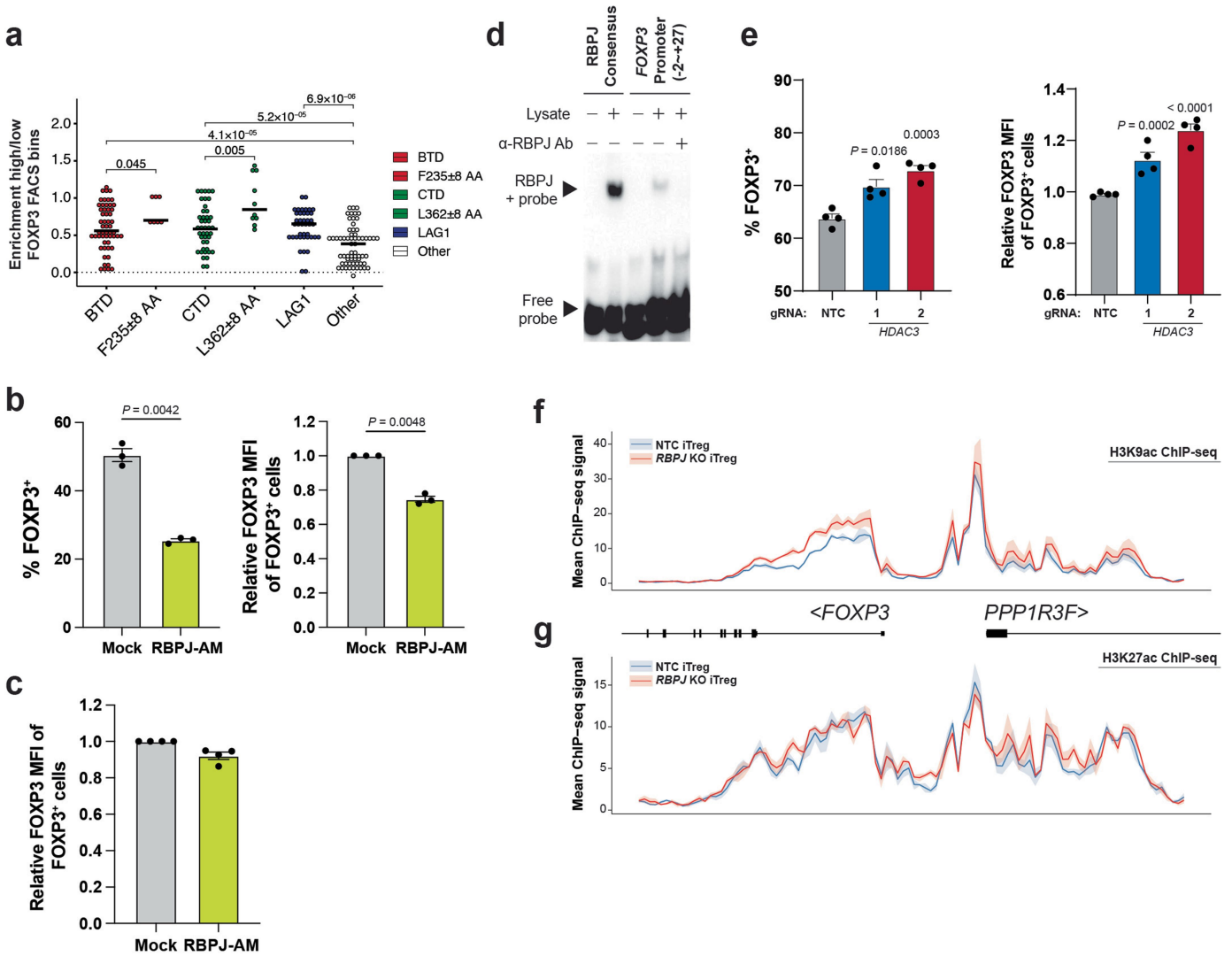

Extended Data Fig. 7 | RBPJ binds to the FOXP3 promoter and modulates histone acetylation. a, Comparison of FOXP3^{hi} versus FOXP3^{lo} gRNA enrichment scores within specific domains, related to the saturation mutagenesis experiment in Fig. 4a. Regions surrounding the amino acid positions 235 and 362 have been removed from the BTD and CTD domains, respectively. BTD, β-trefoil DNA-binding domain; AA, amino acid. *P*-values by a two-tailed Wilcoxon signed-rank test. **b**, RBPJ-overexpressing human CD4$^+$ iTreg cells ($n = 3$ independent donors) were assessed for FOXP3 expression and quantified for %FOXP3$^+$ (left) and FOXP3 MFI (bottom). **c**, RBPJ overexpression has minimal effects on FOXP3 in nTregs, as assessed by flow cytometry ($n = 4$ independent donors). **d**, Electromobility shift assays (EMSA) showing binding of RBPJ to the *FOXP3* promoter. Lysate was prepared from RBPJ-overexpressing iTreg cells (Methods). Data is representative of two independent experiments. **e**, Analysis of %FOXP3$^+$ cells (left) and FOXP3 MFI (right) after iTreg polarization in HDAC3-deficient human CD4$^+$ T cells ($n = 4$ donors). **f**,**g**, Summary of H3K9ac ChIP-seq signal enrichment at *FOXP3*. All data are plotted as ± s.e.m. Repeated measures one-way ANOVA with Dunnett's multiple comparison test for **c**; two-tailed paired Student's *t*-test in **b**. Values plotted in **a** represent CRISPRO gRNA enrichment scores calculated using data from three independent biological replicates.

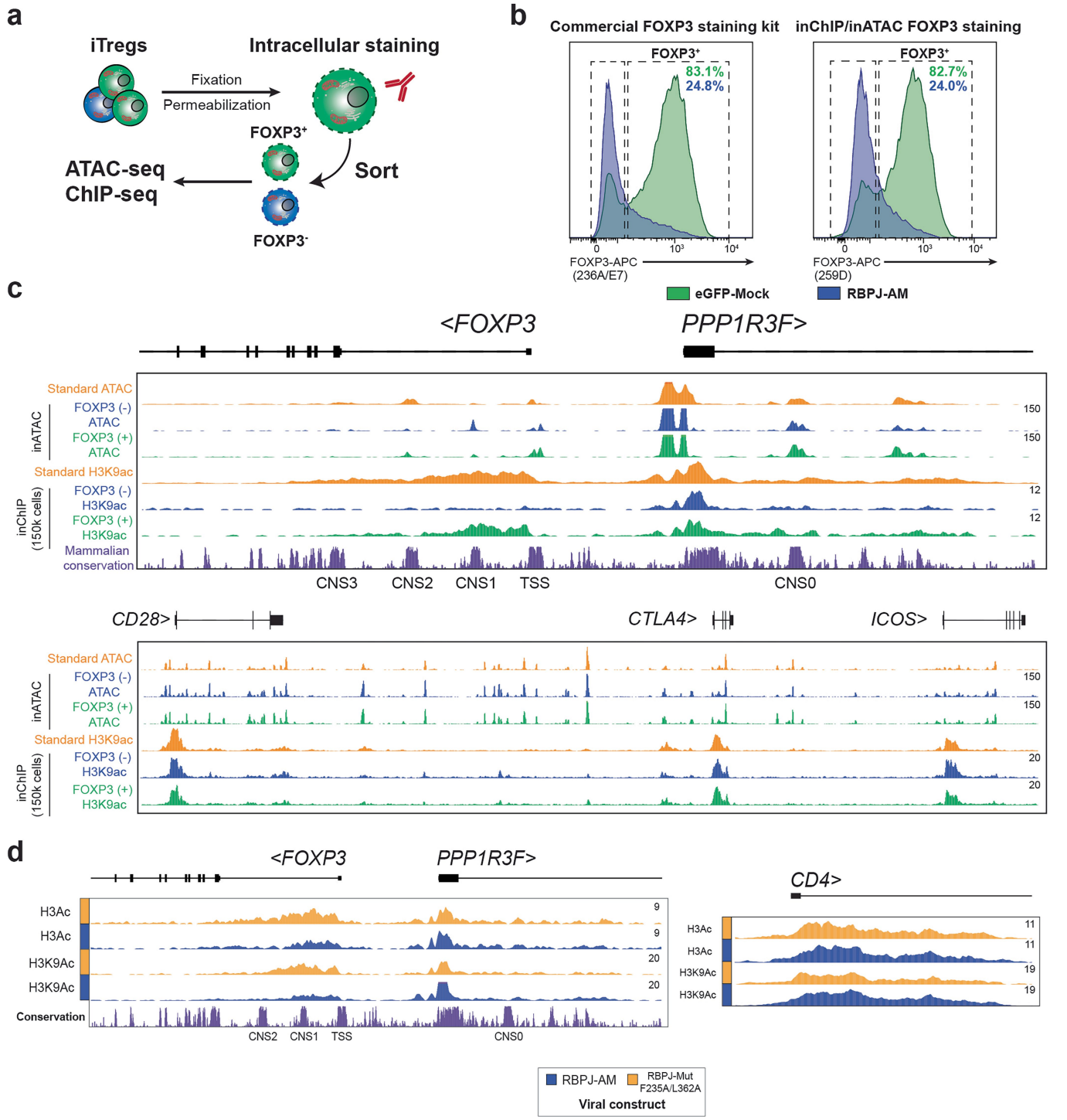

Extended Data Fig. 8 | inChIP and inATAC assessment of chromatin and histone acetylation in FACS-enriched FOXP3$^+$ cells. a, Schematic depicting the inATAC and inChIP protocol (Methods). The schematic was adapted from ref. 51, Springer Nature. **b**, Validation of FOXP3 intracellular staining using the inChIP/inATAC protocol. Comparisons between the two staining protocols were sourced from the same pool of cells. Data is representative of four independent trials and the antibody clones used are indicated. **c**. Genome coverage track of inATAC and inChIP data at the *FOXP3* (Top) and *CTLA4* loci. Data was generated from FACS-sorted FOXP3$^+$ or FOXP3$^-$ iTreg cells and representative of three independent donors. Standard ATAC and Standard H3K9ac tracks were sourced from a separate donor, using a heterogeneous population (FOXP3$^+$ and FOXP3$^-$) of cells. **d**, H3ac and H3K9ac inChIP comparison of FOXP3$^+$ iTregs transduced with WT or mutant RBPJ at the *FOXP3* and *CD4* loci. Results demonstrate that overexpression of WT RBPJ markedly diminishes histone acetylation at *FOXP3*, but not *CD4*.

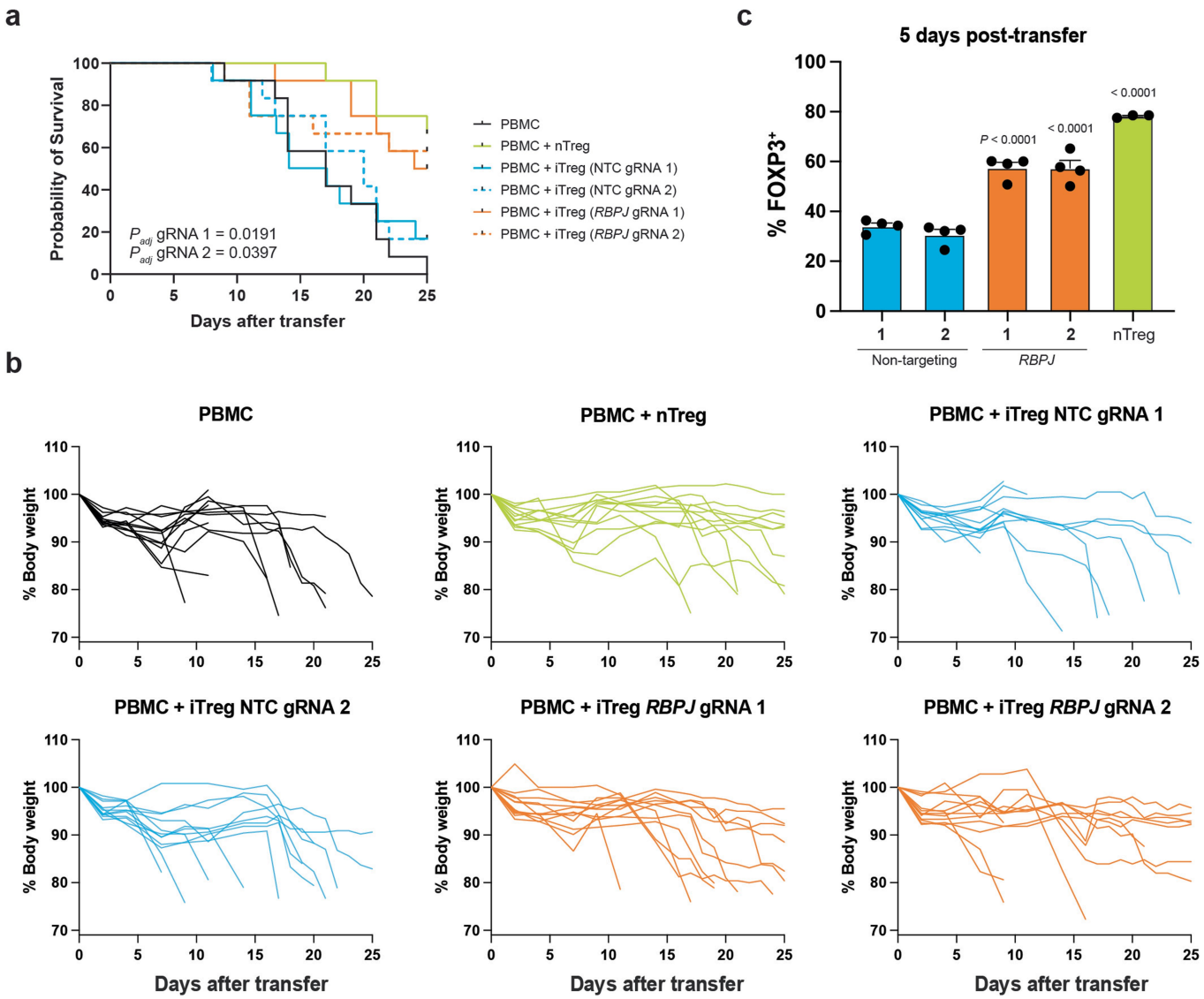

Extended Data Fig. 9 | Supporting information for *RBPJ* ablation improves iTreg in vivo stability and suppressive function. a, Survival curve for the indicated conditions ($n = 12$). Survival *P*-values by log-rank test adjusted for multiple testing. **b**, Relative body weight change of the cohort in **a** over time. **c**, Statistical analysis of FOXP3% in iTregs five days post-transfer ($n = 4$; $n = 3$ for nTregs). Data are presented as mean ± s.e.m., Repeated measures one-way ANOVA with Dunnett's multiple comparison test.

nature portfolio

Corresponding author(s): Kelvin Y. Chen, Shimon Sakaguchi

Last updated by author(s): 2025/01/06

Reporting Summary

Nature Portfolio wishes to improve the reproducibility of the work that we publish. This form provides structure for consistency and transparency in reporting. For further information on Nature Portfolio policies, see our Editorial Policies and the Editorial Policy Checklist.

Statistics

For all statistical analyses, confirm that the following items are present in the figure legend, table legend, main text, or Methods section.

n/a	Confirmed
☐	☒ The exact sample size (*n*) for each experimental group/condition, given as a discrete number and unit of measurement
☐	☒ A statement on whether measurements were taken from distinct samples or whether the same sample was measured repeatedly
☐	☒ The statistical test(s) used AND whether they are one- or two-sided *Only common tests should be described solely by name; describe more complex techniques in the Methods section.*
☐	☒ A description of all covariates tested
☐	☒ A description of any assumptions or corrections, such as tests of normality and adjustment for multiple comparisons
☐	☒ A full description of the statistical parameters including central tendency (e.g. means) or other basic estimates (e.g. regression coefficient) AND variation (e.g. standard deviation) or associated estimates of uncertainty (e.g. confidence intervals)
☐	☒ For null hypothesis testing, the test statistic (e.g. *F*, *t*, *r*) with confidence intervals, effect sizes, degrees of freedom and *P* value noted *Give P values as exact values whenever suitable.*
☒	☐ For Bayesian analysis, information on the choice of priors and Markov chain Monte Carlo settings
☒	☐ For hierarchical and complex designs, identification of the appropriate level for tests and full reporting of outcomes
☐	☒ Estimates of effect sizes (e.g. Cohen's *d*, Pearson's *r*), indicating how they were calculated

Our web collection on statistics for biologists contains articles on many of the points above.

Software and code

Policy information about availability of computer code

Data collection	Flow cytometry data were collected using FACSDiva software (version 9.1, BD Biosciences). For next-generation sequencing data, libraries were sequenced on the Illumina NextSeq500 or NovaSeq6000 (Illumina, USA). Immunoblotting: Image collection was performed on a Jess Automated Western Blot System (ProteinSimple) Compass for SW v6.1.0. EMSA imaging collection was performed on a AI600 Chemiluminescent Imager (Cytiva). Luciferase measurements were collected on a Cytation 5 Cell Imaging Multi-Mode Reader (Agilent). RNA integrity was assed on a 2100 Bioanalyzer System (Agilent Technologies).
Data analysis	Figures were created and statistical tests were performed on Graphpad Prism version 10.4.1. Flow cytometric data was analyzed using FlowJo version 10.10. Custom code to reproduce the scRNA analyses is available at: https://github.com/agiguelay/Perturb-icCITEseq FastQC v0.11.8, CellRanger v7.0.0, Seurat v4.1.2, MIMOSCA, kite v0.02, kallisto v0.44.0, bustools v0.39.3, STAR v2.7.10b, HTSeq-count v2.0.2, fgsea v1.26.0, bowtie2 v2.5.0, deepTools v2.0, CUT&RUNTools v2.0, macs2 v2.2.9.1, samtools v1.17, igraph v1.4.2, MAGeCK v0.5.9.5, CRISPRO v1.0.1, DESeq2 v1.42.1, Trim Galore v0.6.4, kSamples v1.2, multtest v3.2

For manuscripts utilizing custom algorithms or software that are central to the research but not yet described in published literature, software must be made available to editors and reviewers. We strongly encourage code deposition in a community repository (e.g. GitHub). See the Nature Portfolio guidelines for submitting code & software for further information.

Data

Policy information about availability of data

All manuscripts must include a data availability statement. This statement should provide the following information, where applicable:

- Accession codes, unique identifiers, or web links for publicly available datasets
- A description of any restrictions on data availability
- For clinical datasets or third party data, please ensure that the statement adheres to our policy

All CRISPR screen data generated for this manuscript is provided in Supplementary Tables 1 and 4.
Raw sequencing data for ChIP-seq, ATAC-seq, CUT&RUN, inATAC-seq, inChIP-seq, Perturb-icCITE-seq, RNA-seq and icRNA-seq have been deposited in the DNA Data Bank of Japan Sequence Read Archive (DDBJ) and are accessible through the accession number PRJDB16517.

All data aligned to human reference GRCh38 (hg38).

Research involving human participants, their data, or biological material

Policy information about studies with human participants or human data. See also policy information about sex, gender (identity/presentation), and sexual orientation and race, ethnicity and racism.

Reporting on sex and gender	For experiments involving bisulfite sequencing of the FOXP3 locus, only male donors were used to avoid random X-inactivation.
Reporting on race, ethnicity, or other socially relevant groupings	Race, ethnicity, and other social grouping were not deemed as relevant variables for the purpose of this study.
Population characteristics	Peripheral blood mononuclear cells (PBMCs) or cord blood from anonymous healthy humans (male and female, no age specified) were purchased from Cellular Technology Limited, Lonza or STEMCELL Technologies. New T cell donors were ordered regularly and different experiments used different T cell donors.
Recruitment	PBMC and cord blood were purchased from Cellular Technology Limited, Lonza and STEMCELL Technologies
Ethics oversight	The PBMCs and cord blood were purchased from Cellular Technology Limited, Lonza or STEMCELL Technologies, which collect from healthy donors under protocols approved by the Cellular Technology Limited IRB, the Lonza IRB or the STEMCELL Technologies IRB.

Note that full information on the approval of the study protocol must also be provided in the manuscript.

Field-specific reporting

Please select the one below that is the best fit for your research. If you are not sure, read the appropriate sections before making your selection.

☒ Life sciences ☐ Behavioural & social sciences ☐ Ecological, evolutionary & environmental sciences

For a reference copy of the document with all sections, see nature.com/documents/nr-reporting-summary-flat.pdf

Life sciences study design

All studies must disclose on these points even when the disclosure is negative.

Sample size	No statistical methods were used to predetermine sample size. Sample size is stated in each panel, including number of independent human donors. Group sizes were validated by experienced with well-established, previously published models (1-3). 1) Mikami, N. et al. Epigenetic conversion of conventional T cells into regulatory T cells by CD28 signal deprivation. Proc. Natl. Acad. Sci. U. S. A. 117, (2020). 2) Cortez, J. T. et al. CRISPR screen in regulatory T cells reveals modulators of Foxp3. Nature 582, (2020). 3) Hippen, K. L. et al. Generation and large-scale expansion of human inducible regulatory T cells that suppress graft-versus-host disease. American journal of transplantation : official journal of the American Society of Transplantation and the American Society of Transplant Surgeons 11, (2011).
Data exclusions	No data were excluded from the analysis.
Replication	Each experiment was reproduced at least twice to confirm reproducibility.
Randomization	For experiments that require treatments, age- and sex-matched animals were randomly assigned into each group. For in vitro experiments, no randomizing was required as each condition was controlled within each donor.
Blinding	In vitro experiments were not performed in a blinded fashion, but were measured with objective methodologies. For in vivo experiments, measurements of weight loss and monitoring of mouse health were performed by an experimenter blinded to the experimental groups.

Reporting for specific materials, systems and methods

We require information from authors about some types of materials, experimental systems and methods used in many studies. Here, indicate whether each material, system or method listed is relevant to your study. If you are not sure if a list item applies to your research, read the appropriate section before selecting a response.

Materials & experimental systems

n/a	Involved in the study
☐	☒ Antibodies
☐	☒ Eukaryotic cell lines
☒	☐ Palaeontology and archaeology
☐	☒ Animals and other organisms
☒	☐ Clinical data
☒	☐ Dual use research of concern
☒	☐ Plants

Methods

n/a	Involved in the study
☐	☒ ChIP-seq
☐	☒ Flow cytometry
☒	☐ MRI-based neuroimaging

Antibodies

Antibodies used

For Flow Cytometry (epitope-clone-fluorophore-vendor-catalog#-dilution):
hCD2 RPA-2.10 APC BioLegend 300213 1:100
hCD2 RPA-2.10 FITC BioLegend 300206 1:100
hCD4 RPA-T4 BV510 BD 740161 1:100
hCD4 RPA-T4 PerCP-Cy5.5 BD 560650 1:100
hCD4 RPA-T4 APC BD 555349 1:100
hCD8 HIT8a APC BD 566852 1:100
hCD16 3G8 FITC BD 560996 1:100
hCD25 M-A251 PE BD 555432 1:10
hCD127 HIL-7R-M21 BV786 BD 563324 1:50
hCD45RA HI100 APC BioLegend 304112 1:50
hCTLA-4 BNI3 BV421 BD 562743 1:100
hFoxP3 236A/E7 PE Invitrogen 12-4777-42 1:100
hFoxP3 236A/E7 APC Invitrogen 17-4777-42 1:100
hFoxP3 259D AF647 BioLegend 320214 1:50
mCD45 30-F11 BV510 BD 563891 1:100
mCD4 RM4-5 BV421 Invitrogen 404-0042-82 1:100
mFoxp3 FJK-16s PE Invitrogen 12-5773-82 1:100
mCD90.1 (Thy-1.1) OX-7 AF647 BioLegend 202508 1:100
mCD62L MEL-14 APC Invitrogen 17-0621-83 1:100
mCD44 IM7 PE-Cy7 Invitrogen 25-0441-82 1:100

For EMSA (epitope-clone-vendor-catalog#-dilution):
anti-RBPJ 1F1 Active Motif 61505 10 ng/mL

For Immunoblotting (epitope-clone-vendor-catalog#-dilution):
AbFlex® AM-Tag antibody Active Motif 91111 5 µg
IgG2a isotype control 6H3 MBL M076-3 5 µg
anti-NCOR2 D8D2L CST 62370 1:50
anti-RBPJ EPR13479 Abcam ab180588 1:50
anti-HDAC3 D2O1K CST 85057S 1:50

For in-house icCITE-seq conjugations(epitope-clone-vendor-catalog#):
Phospho-p38 MAPK (Thr180/Tyr182) D3F9 CST 4511S
Phospho-NF-κB p65 (Ser536) 93H1 CST 3033S
Phospho-cJun (Ser73) D47G9 CST 3270S
BCL11B 25B6 Absolute antibody Ab00616-23.0
phospho-Stat3_Tyr705_D3A7 D3A7 CST 9145S
Phospho-SLP-76 (Ser376) E3G9U CST 76384S
Phospho-MEK1 (pS298) J114-64 BD 558375
RORGT REA278 Milltenyi 130-108-059
pSTAT5 Y694 47/Stat5(pY694) BD 611964
RUNX1 D33G6 CST 4336S
GATA3 REA174 Milltenyi 130-108-061
Phospho-p44/42 MAPK (Erk1/2) (Thr202/Tyr204) 197G2 CST 4377S

Custom purified sourced from BD)
Phospho-LAT (pY226) J96-1238.58.93
Phospho-CREB (pS133) / ATF-1 (pS63) J151-21
RUNX3 R3-5G4

CITE-seq antibodies (BioLegend): A list of antibodies included in Supplementary Table 6 - 'icCITE surface panel'
Hashtag antibodies (BioLegend): A list of antibodies included in Supplementary Table 6 - 'icCITE Hashtag antibodies'
icCITE-seq intracellular antibodies: list of antibodies included in Supplementary Table 6 - 'icCITE intracellular panel'

ChIP-seq/inChIP-seq/CUT&RUN antibodies:
H3ac Polyclonal Millipore 06-599
H3K9ac Polyclonal Abcam ab4441
H3K27ac Polyclonal Abcam ab4729
IgG2a isotype control 6H3 MBL M076-3
AbFlex® AM-Tag antibody Active Motif 91111

Validation

All flow cytometry antibodies were validated by the manufacturers using various human peripheral blood mononuclear cells or mouse splenocytes. Further validation was conducted at Osaka University, where antibody-specific staining was compared against isotype controls and unstained samples.

Western blot were validated by manufacturers on cell lines as noted below in the specific antibody sections.
In-house conjugated intracellular icCITE-seq antibodies were validated for flow cytometry by the manufacturers as indicated.

Antibody validation can be found at the following sites:

hCD2 RPA-2.10 APC BioLegend 300213
https://www.biolegend.com/en-us/products/apc-anti-human-cd2-antibody-7219

hCD2 RPA-2.10 FITC BioLegend 300206
https://www.biolegend.com/en-us/products/fitc-anti-human-cd2-antibody-818

hCD4 RPA-T4 BV510 BD 740161
https://www.bdbiosciences.com/en-us/products/reagents/flow-cytometry-reagents/research-reagents/single-color-antibodies-ruo/bv510-mouse-anti-human-cd4.740161?tab=product_details

hCD4 RPA-T4 PerCP-Cy5.5 BD 560650
https://www.bdbiosciences.com/en-us/products/reagents/flow-cytometry-reagents/research-reagents/single-color-antibodies-ruo/percp-cy-5-5-mouse-anti-human-cd4.560650?tab=product_details

hCD4 RPA-T4 APC BD 555349
https://www.bdbiosciences.com/en-us/products/reagents/flow-cytometry-reagents/research-reagents/single-color-antibodies-ruo/apc-mouse-anti-human-cd4.555349?tab=product_details

hCD8 HIT8a APC BD 566852
https://www.bdbiosciences.com/en-us/products/reagents/flow-cytometry-reagents/research-reagents/single-color-antibodies-ruo/apc-mouse-anti-human-cd8.566852?tab=product_details

hCD16 3G8 FITC BD 560996
https://www.bdbiosciences.com/en-us/products/reagents/flow-cytometry-reagents/research-reagents/single-color-antibodies-ruo/fitc-mouse-anti-human-cd16.560996?tab=product_details

hCD25 M-A251 PE BD 555432
https://www.bdbiosciences.com/en-us/products/reagents/flow-cytometry-reagents/research-reagents/single-color-antibodies-ruo/pe-mouse-anti-human-cd25.555432?tab=product_details

hCD127 HIL-7R-M21 BV786 BD 563324
https://www.bdbiosciences.com/en-us/products/reagents/flow-cytometry-reagents/research-reagents/single-color-antibodies-ruo/bv786-mouse-anti-human-cd127.563324?tab=product_details

hCD45RA HI100 APC BioLegend 304112
https://www.biolegend.com/en-us/products/apc-anti-human-cd45ra-antibody-684?GroupID=GROUP658

hCTLA-4 BNI3 BV421 BD 562743
https://www.bdbiosciences.com/en-eu/products/reagents/flow-cytometry-reagents/research-reagents/single-color-antibodies-ruo/bv421-mouse-anti-human-cd152.562743?tab=product_details

hFoxP3 236A/E7 PE Invitrogen 12-4777-42
https://www.thermofisher.com/antibody/product/FOXP3-Antibody-clone-236A-E7-Monoclonal/12-4777-42

hFoxP3 236A/E7 APC Invitrogen 17-4777-42
https://www.thermofisher.com/antibody/product/FOXP3-Antibody-clone-236A-E7-Monoclonal/17-4777-42

hFoxP3 259D AF647 BioLegend 320214
https://www.biolegend.com/en-us/products/alexa-fluor-647-anti-human-foxp3-antibody-2909

mCD45 30-F11 BV510 BD 563891
https://www.bdbiosciences.com/en-us/products/reagents/flow-cytometry-reagents/research-reagents/single-color-antibodies-ruo/bv510-rat-anti-mouse-cd45.563891?tab=product_details

mCD4 RM4-5 BV421 Invitrogen 404-0042-82

https://www.thermofisher.com/antibody/product/CD4-Antibody-clone-RM4-5-Monoclonal/404-0042-82

mFoxp3 FJK-16s PE Invitrogen 12-5773-82
https://www.thermofisher.com/antibody/product/FOXP3-Antibody-clone-FJK-16s-Monoclonal/12-5773-82

mCD90.1 (Thy-1.1) OX-7 AF647 BioLegend 202508
https://www.biolegend.com/en-us/products/alexa-fluor-647-anti-rat-cd90-mouse-cd90-1-thy-1-1-antibody-3127?GroupID=BLG10566

mCD62L MEL-14 APC Invitrogen 17-0621-83
https://www.thermofisher.com/antibody/product/CD62L-L-Selectin-Antibody-clone-MEL-14-Monoclonal/17-0621-83

mCD44 IM7 PE-Cy7 Invitrogen 25-0441-82
https://www.thermofisher.com/antibody/product/CD44-Antibody-clone-IM7-Monoclonal/25-0441-82

anti-RBPJ 1F1 Active Motif 61505 - Validated on HeLa cells
https://www.activemotif.jp/catalog/details/61505/rbpj-antibody-mab-clone-1f1

AbFlex® AM-Tag antibody 91111 - Validated on HCT116 cells
https://www.activemotif.com/catalog/details/91111

IgG2a isotype control 6H3 MBL M076-3 - Validated on Jurkat cells, 293T cells and whole blood cells
https://ruo.mbl.co.jp/bio/dtl/A/?pcd=M076-3

anti-RBPJ EPR13479 Abcam ab180588 - Validated on Raji, MCF7, F9, C6, 293T, HEK-293, PC-12, NIH/3T3, Raw264.7, and HeLa cells
https://www.abcam.com/en-us/products/primary-antibodies/rbpjk-antibody-epr13479-ab180588

anti-HDAC3 D2O1K CST 85057S - Validated on MCF7, NIH/3T3, H-4II-E, and COS-7 cells
https://www.cellsignal.jp/products/primary-antibodies/hdac3-d2o1k-rabbit-mab/85057

Phospho-p38 MAPK (Thr180/Tyr182) D3F9 CST - Validated on Jurkat cells
https://www.cellsignal.jp/products/primary-antibodies/phospho-p38-mapk-thr180-tyr182-d3f9-xp-rabbit-mab/4511

Phospho-NF-κB p65 (Ser536) 93H1 CST - Validated on HeLa cells
https://www.cellsignal.jp/products/primary-antibodies/phospho-nf-kb-p65-ser536-93h1-rabbit-mab/3033

Phospho-cJun (Ser73) D47G9 CST - Validated on HeLa cells
https://www.cellsignal.jp/products/primary-antibodies/phospho-c-jun-ser73-d47g9-xp-rabbit-mab/3270

BCL11B 25B6 Absolute antibody Ab00616-23.0 - Validated on Neuro-2a cells
https://absoluteantibody.com/product/anti-ctip2-25b6/

Phospho-LAT (pY226) J96-1238.58.93 BD - Validated on Jurkat cells
https://www.bdbiosciences.com/en-us/products/reagents/flow-cytometry-reagents/research-reagents/single-color-antibodies-ruo/pe-mouse-anti-lat-py226.558433?tab=product_details

Phospho-CREB (pS133) / ATF-1 (pS63) J151-21 BD - Validated on human peripheral blood lymphocytes
https://www.bdbiosciences.com/en-us/products/reagents/flow-cytometry-reagents/research-reagents/single-color-antibodies-ruo/pe-mouse-anti-creb-ps133-atf-1-ps63.558436?tab=product_details

phospho-Stat3_Tyr705_D3A7 D3A7 CST - Validated on U266 cells
https://www.cellsignal.jp/products/primary-antibodies/phospho-stat3-tyr705-d3a7-xp-rabbit-mab/9145

Phospho-SLP-76 (Ser376) E3G9U CST - Validated on human peripheral blood mononuclear cells
https://www.cellsignal.jp/products/primary-antibodies/phospho-slp-76-ser376-e3g9u-xp-rabbit-mab/76384

Phospho-MEK1 (pS298) J114-64 BD - Validated on Hela S3 cells
https://www.bdbiosciences.com/en-no/products/reagents/western-blotting-and-molecular-reagents/western-blot-reagents/purified-mouse-anti-mek1-ps298.558375?tab=product_details

RORGT REA278 Milltenyi 130-108-059 - Validated on Mouse thymocytes
https://www.miltenyibiotec.com/JP-en/products/rorg-t-antibody-anti-human-mouse-reafinity-rea278.html#conjugate=vio-b515:size=100-tests-in-200-ul

RUNX3 R3-5G4 BD - Validated on Human PBMC and mouse lymph node cells
https://www.bdbiosciences.com/en-eu/products/reagents/flow-cytometry-reagents/research-reagents/single-color-antibodies-ruo/pe-mouse-anti-runx3.564814?tab=product_details

pSTAT5 Y694 47/Stat5(pY694) BD 611964 - Validated on stimulated human lymphocytes
https://www.bdbiosciences.com/ja-jp/products/reagents/western-blotting-and-molecular-reagents/western-blot-reagents/purified-mouse-anti-human-stat5-py694.611964?tab=product_details

RUNX1 D33G6 CST - Validated on Jurkat cells
https://www.cellsignal.jp/products/primary-antibodies/aml1-d33g6-xp-rabbit-mab/4336

GATA3 REA174 Milltenyi 130-108-061 - Validated on Mouse splenocytes

https://www.miltenyibiotec.com/JP-en/products/gata3-antibody-anti-human-mouse-reafinity-rea174.html#conjugate=pure:size=100-ug-in-100-ul

Phospho-p44/42 MAPK (Erk1/2) (Thr202/Tyr204) 197G2 CST - Validated on Jurkat cells
https://www.cellsignal.jp/products/primary-antibodies/phospho-p44-42-mapk-erk1-2-thr202-tyr204-197g2-rabbit-mab/4377

CITE-seq antibodies (BioLegend): TotalSeq-A Custom Human Universal Cocktail and Hashtag antibodies have been validated by manufacturer.
icCITE-seq antibodies (BioLegend): TotalSeq-B antibodies have been validated by manufacturer.

ChIP/CUT&RUN antibodies were validated by the manufacturer. Please refer to the manufacturer website for detailed validation analysis. Antibodies were also validted by our laboratory by ChIP-seq/CUT&RUN (specific peaks).

H3ac Polyclonal Millipore 06-599
https://www.emdmillipore.com/US/en/product/Anti-acetyl-Histone-H3-Antibody,MM_NF-06-599?ReferrerURL=https%3A%2F%2Fwww.google.com%2F&bd=1

H3K9ac Polyclonal Abcam ab4441
https://www.abcam.com/en-us/products/primary-antibodies/histone-h3-acetyl-k9-antibody-chip-grade-ab4441
H3K27ac Polyclonal Abcam ab4729
https://www.abcam.com/en-us/products/primary-antibodies/histone-h3-acetyl-k27-antibody-chip-grade-ab4729

IgG2a isotype control 6H3 MBL M076-3
https://ruo.mbl.co.jp/bio/e/dtl/A/?pcd=M076-3

AbFlex® AM-Tag antibody Active Motif 91111
https://www.activemotif.com/catalog/details/91111

Eukaryotic cell lines

Policy information about cell lines and Sex and Gender in Research

Cell line source(s)	Lenti-X 293T cells were obtained from Takara Bio. PLAT-E cells were obtained from Dr. Toshio Kitamura and are commercially available from from Cell BioLabs, Inc.
Authentication	Lenti-X 293T cells were authenticated from the original vendor. PLAT-E cells were authenticated by Dr. Toshio Kitamura. Both cell lines were also authenticated in-house by morphology and viral particle-producing ability (functional titer).
Mycoplasma contamination	The aforementioned lines were not tested, but other lines used in the same hood/incubator have been routinely tested and have always been negative.
Commonly misidentified lines (See ICLAC register)	No misidentified cell lines were used in this study.

Animals and other research organisms

Policy information about studies involving animals; ARRIVE guidelines recommended for reporting animal research, and Sex and Gender in Research

Laboratory animals	B6.Foxp3-hCD2/CD4-Cre mice were crossed with H11-LSL-Cas9 mice to generate Foxp3-hCD2/H11-LSL-Cas9/CD4-Cre mice used for the murine validation experiments. H11-LSL-Cas9 (Jackson #026816) and CD4-Cre (Jackson #022071) mice were purchased from The Jackson Laboratory. The Rbpj flox/flox mouse strain (RBRC01071) was provided by RIKEN BRC through the National BioResource Project of the MEXT/AMED, Japan and crossed with Foxp3-hCD2 to generate B6/Rbpj flox/flox Foxp3-hCD2 mice. NSG mice were purchased from Jackson Laboratory. Mice were housed at the Animal Resource Center for Infectious Diseases of Osaka University with a 12-h light–dark cycle, and mice were kept at a temperature of 21.5–24.5 °C with humidity ranging from 30–60%. Male mice between the age of 6-7 weeks were used.
Wild animals	No wild animals were used in the study.
Reporting on sex	Only male mice were used for genetic reasons.
Field-collected samples	No field collected samples were used in the study.
Ethics oversight	All procedures were performed in accordance with the National Institutes of Health Guide for the Care and Use of Laboratory Animals and approved by the Committee on Animal Research of Osaka University.

Note that full information on the approval of the study protocol must also be provided in the manuscript.

Plants

Seed stocks

Report on the source of all seed stocks or other plant material used. If applicable, state the seed stock centre and catalogue number. If plant specimens were collected from the field, describe the collection location, date and sampling procedures.

Novel plant genotypes

Describe the methods by which all novel plant genotypes were produced. This includes those generated by transgenic approaches, gene editing, chemical/radiation-based mutagenesis and hybridization. For transgenic lines, describe the transformation method, the number of independent lines analyzed and the generation upon which experiments were performed. For gene-edited lines, describe the editor used, the endogenous sequence targeted for editing, the targeting guide RNA sequence (if applicable) and how the editor was applied.

Authentication

Describe any authentication procedures for each seed stock used or novel genotype generated. Describe any experiments used to assess the effect of a mutation and, where applicable, how potential secondary effects (e.g. second site T-DNA insertions, mosiacism, off-target gene editing) were examined.

ChIP-seq

Data deposition

☒ Confirm that both raw and final processed data have been deposited in a public database such as GEO.

☒ Confirm that you have deposited or provided access to graph files (e.g. BED files) for the called peaks.

Data access links
May remain private before publication.

Raw sequencing data has been deposited in the DNA Data Bank of Japan Sequence Read Archive (DDBJ) and are accessible through the accession number PRJDB16517.

Files in database submission

inChIP_H3ac_Foxp3nega_D1.SeqDepthNorm.bw
inChIP_H3ac_Foxp3nega_D2.SeqDepthNorm.bw
inChIP_H3ac_Foxp3nega_D3.SeqDepthNorm.bw
inChIP_H3ac_Foxp3posi_D1.SeqDepthNorm.bw
inChIP_H3ac_Foxp3posi_D2.SeqDepthNorm.bw
inChIP_H3ac_Foxp3posi_D3.SeqDepthNorm.bw
inChIP_H3ac_Foxp3posi_RBPJ_MT_D4.SeqDepthNorm.bw
inChIP_H3ac_Foxp3posi_RBPJ_MT_D5.SeqDepthNorm.bw
inChIP_H3ac_Foxp3posi_RBPJ_WT_D2.SeqDepthNorm.bw
inChIP_H3ac_Foxp3posi_RBPJ_WT_D3.SeqDepthNorm.bw
inChIP_H3ac_Foxp3posi_RBPJ_WT_D4.SeqDepthNorm.bw
inChIP_H3ac_Foxp3posi_RBPJ_WT_D5.SeqDepthNorm.bw
inChIP_H3K9ac_Foxp3nega_D1.SeqDepthNorm.bw
inChIP_H3K9ac_Foxp3nega_D2.SeqDepthNorm.bw
inChIP_H3K9ac_Foxp3posi_D1.SeqDepthNorm.bw
inChIP_H3K9ac_Foxp3posi_D2.SeqDepthNorm.bw
inChIP_H3K9ac_Foxp3posi_RBPJ_MT_D2.SeqDepthNorm.bw
inChIP_H3K9ac_Foxp3posi_RBPJ_MT_D3.SeqDepthNorm.bw
inChIP_H3K9ac_Foxp3posi_RBPJ_WT_D1.SeqDepthNorm.bw
inChIP_H3K9ac_Foxp3posi_RBPJ_WT_D2.SeqDepthNorm.bw
inChIP_H3K9ac_Foxp3posi_RBPJ_WT_D3.SeqDepthNorm.bw
ChIP_0304_NTC_H3ac_D2.macs2_peaks.narrowPeak
ChIP_0304_NTC_H3ac_D2.SeqDepthNorm.bw
ChIP_0304_NTC_H3K27ac_D2.macs2_peaks.narrowPeak
ChIP_0304_NTC_H3K27ac_D2.SeqDepthNorm.bw
ChIP_0304_NTC_H3K9ac_D2.macs2_peaks.narrowPeak
ChIP_0304_NTC_H3K9ac_D2.SeqDepthNorm.bw
ChIP_0304_RBPJ_KO_H3ac_D2.macs2_peaks.narrowPeak
ChIP_0304_RBPJ_KO_H3ac_D2.SeqDepthNorm.bw
ChIP_0304_RBPJ_KO_H3K27ac_D2.macs2_peaks.narrowPeak
ChIP_0304_RBPJ_KO_H3K27ac_D2.SeqDepthNorm.bw
ChIP_0304_RBPJ_KO_H3K9ac_D2.macs2_peaks.narrowPeak
ChIP_0304_RBPJ_KO_H3K9ac_D2.SeqDepthNorm.bw
ChIP_0309_NTC_H3ac_D1.macs2_peaks.narrowPeak
ChIP_0309_NTC_H3ac_D1.SeqDepthNorm.bw
ChIP_0309_NTC_H3K27ac_D1.macs2_peaks.narrowPeak
ChIP_0309_NTC_H3K27ac_D1.SeqDepthNorm.bw
ChIP_0309_NTC_H3K9ac_D1.macs2_peaks.narrowPeak
ChIP_0309_NTC_H3K9ac_D1.SeqDepthNorm.bw
ChIP_0309_RBPJ_KO_H3ac_D1.macs2_peaks.narrowPeak
ChIP_0309_RBPJ_KO_H3ac_D1.SeqDepthNorm.bw
ChIP_0309_RBPJ_KO_H3K27ac_D1.macs2_peaks.narrowPeak
ChIP_0309_RBPJ_KO_H3K27ac_D1.SeqDepthNorm.bw
ChIP_0309_RBPJ_KO_H3K9ac_D1.macs2_peaks.narrowPeak
ChIP_0309_RBPJ_KO_H3K9ac_D1.SeqDepthNorm.bw
ChIP_0316_NTC_H3ac_D3.macs2_peaks.narrowPeak
ChIP_0316_NTC_H3ac_D3.SeqDepthNorm.bw

ChIP_0316_NTC_H3K27ac_D3.macs2_peaks.narrowPeak
ChIP_0316_NTC_H3K27ac_D3.SeqDepthNorm.bw
ChIP_0316_NTC_H3K9ac_D3.macs2_peaks.narrowPeak
ChIP_0316_NTC_H3K9ac_D3.SeqDepthNorm.bw
ChIP_0316_RBPJ_KO_H3ac_D3.macs2_peaks.narrowPeak
ChIP_0316_RBPJ_KO_H3ac_D3.SeqDepthNorm.bw
ChIP_0316_RBPJ_KO_H3K27ac_D3.macs2_peaks.narrowPeak
ChIP_0316_RBPJ_KO_H3K27ac_D3.SeqDepthNorm.bw
ChIP_0316_RBPJ_KO_H3K9ac_D3.macs2_peaks.narrowPeak
ChIP_0316_RBPJ_KO_H3K9ac_D3.SeqDepthNorm.bw
CR_anti-AM_RBPJ_MT_D3.cpm.norm.bw
CR_anti-AM_RBPJ_MT_D4.cpm.norm.bw
CR_anti-AM_RBPJ_WT_D1.cpm.norm.bw
CR_anti-AM_RBPJ_WT_D2.cpm.norm.bw
CR_anti-AM_RBPJ_WT_D5.cpm.norm.bw
CR_anti-IgG_RBPJ_MT_D3.cpm.norm.bw
CR_anti-IgG_RBPJ_MT_D4.cpm.norm.bw
CR_anti-IgG_RBPJ_WT_D1.cpm.norm.bw
CR_anti-IgG_RBPJ_WT_D2.cpm.norm.bw
CR_anti-IgG_RBPJ_WT_D5.cpm.norm.bw

Genome browser session (e.g. UCSC): no longer applicable

Methodology

Replicates: A minimum of two biological replicates from independent donors were performed.

Sequencing depth: All samples were sequenced as paired-end reads with a minimum read-length of 50 bp.

Antibodies:
Anti-acetyl-Histone H3 Antibody - Millipore; Polyclonal; 06-599
Anti-Histone H3 (acetyl K9) antibody - Abcam; Polyclonal; ab4441
Anti-Histone H3 (acetyl K27) antibody - Abcam; Polyclonal; ab4729
IgG2a isotype control - MBL; 6H3; M076-3
AbFlex® AM-Tag antibody - Active Motif; 91111

Peak calling parameters: Peaks were called using CUT&RUNTools v2.0 and macs2 v2.2.9.1 under default parameters.

Data quality: Raw sequencing quality was assessed by FastQC.

Software: bowtie2 v2.5.0, deepTools v2.0, CUT&RUNTools v2.0, macs2 v2.2.9.1, samtools v1.17, FastQC v0.11.8

Flow Cytometry

Plots

Confirm that:

☒ The axis labels state the marker and fluorochrome used (e.g. CD4-FITC).

☒ The axis scales are clearly visible. Include numbers along axes only for bottom left plot of group (a 'group' is an analysis of identical markers).

☒ All plots are contour plots with outliers or pseudocolor plots.

☒ A numerical value for number of cells or percentage (with statistics) is provided.

Methodology

Sample preparation: Cells were stained with appropriate antibodies for cell surface proteins and Live/Dead dye. Cells were fixed and permeabilized using the Foxp3/Transcription Factor Staining Buffer Set (Thermo Fisher), followed by intracellular staining.

Instrument: BD FACSCelesta, BD FACSAria III and BD FACSAria Fusion

Software: FlowJo v10.8.1 and BD FACSDiva v8

Cell population abundance: After sorting, the sorted population was at least 98% pure as confirmed by flow cytometry.

Gating strategy: The gated population is indicated in the text. For all experiments, the population was first gated on FSC/SSC for lymphocytes. Doublets and dead cells were excluded.

☒ Tick this box to confirm that a figure exemplifying the gating strategy is provided in the Supplementary Information.